Activation of conventional kinesin motors in clusters by Shaw voltage-gated K^+ channels

Joshua Barry[1], Mingxuan Xu[2,*], Yuanzheng Gu[2], Andrew W. Dangel[3], Peter Jukkola[4], Chandra Shrestha[2,‡] and Chen Gu[1,2,4,§]

[1]Molecular, Cellular and Developmental Biology Graduate Program, The Ohio State University, Columbus, OH 43210, USA
[2]Department of Neuroscience, The Ohio State University, Columbus, OH 43210, USA
[3]Plant-Microbe Genomics Facility, The Ohio State University, Columbus, OH 43210, USA
[4]Integrated Biomedical Graduate Program, The Ohio State University, Columbus, OH 43210, USA

*Present address: Department of Neurology, Baylor College of Medicine, Houston, TX 77030, USA
‡Present address: Department of Biomedical Sciences and Pathobiology, College of Veterinary Medicine, Virginia Tech University, Blacksburg, VA 24061, USA
§Author for correspondence (gu.49@osu.edu)

Accepted 19 February 2013
Journal of Cell Science 126, 2027–2041

doi: 10.1242/jcs.122234

Summary

The conventional kinesin motor transports many different cargos to specific locations in neurons. How cargos regulate motor function remains unclear. Here we focus on KIF5, the heavy chain of conventional kinesin, and report that the Kv3 (Shaw) voltage-gated K^+ channel, the only known tetrameric KIF5-binding protein, clusters and activates KIF5 motors during axonal transport. Endogenous KIF5 often forms clusters along axons, suggesting a potential role of KIF5-binding proteins. Our biochemical assays reveal that the high-affinity multimeric binding between the Kv3.1 T1 domain and KIF5B requires three basic residues in the KIF5B tail. Kv3.1 T1 competes with the motor domain and microtubules, but not with kinesin light chain 1 (KLC1), for binding to the KIF5B tail. Live-cell imaging assays show that four KIF5-binding proteins, Kv3.1, KLC1 and two synaptic proteins SNAP25 and VAMP2, differ in how they regulate KIF5B distribution. Only Kv3.1 markedly increases the frequency and number of KIF5B-YFP anterograde puncta. Deletion of Kv3.1 channels reduces KIF5 clusters in mouse cerebellar neurons. Therefore, clustering and activation of KIF5 motors by Kv3 regulate the motor number in carrier vesicles containing the channel proteins, contributing not only to the specificity of Kv3 channel transport, but also to the cargo-mediated regulation of motor function.

Key words: Voltage-gated potassium channel, Molecular motor, Axonal transport, Cargo-motor interaction, Kinesin light chain, Synaptic protein

Introduction

Crucial for neuronal functions, membrane proteins including ion channels and receptors are localized to distinct subcellular compartments. Intracellular forward transport of proteins and organelles over long distances is thought to primarily rely on kinesin motors, which distinguish between different microtubules that lead to axons and dendrites (Nakata et al., 2011; Burack et al., 2000; Hirokawa and Takemura, 2005). Other cytoskeletal and associated proteins also regulate the specificity of kinesin-mediated transport. For instance, ankyrin-G and actin filaments at the axon initial segment appear to be critical for maintaining the axon-dendrite polarity by regulating selective transport (Maniar et al., 2012; Xu et al., 2010; Xu et al., 2007; Sobotzik et al., 2009; Song et al., 2009). However, whether cargos themselves can play an important role during selective transport, knowing exactly which motor protein to ride, how to ride, and where to go, still remains unclear.

As a major anterograde motor operating in axons, conventional kinesin-1 consists of a heavy chain (KIF5) dimer and two KLCs binding to the C-termini of the dimer. Although one motor complex is often sufficient to transport one vesicle along a microtubule, a few motors can work together to increase the processivity and travel distance, but not the velocity (Miller and Lasek, 1985; Howard et al., 1989; Block et al., 1990; Hirokawa et al., 1991; Leopold et al., 1992; Schnitzer and Block, 1997; Vershinin et al., 2007; Shubeita et al., 2008; Laib et al., 2009). How the motor number on a carrier vesicle is regulated remains unknown. Furthermore, many proteins directly bind to the KIF5 C-terminal tail domains (Xu et al., 2010), leading to an apparent conundrum for specific recognition and transport of axonal proteins and organelles. How does KIF5 distinguish different cargos, particularly those binding to overlapping sites?

Axonal Kv channels regulate action potential initiation, waveform, frequency and uni-directional propagation along axons, and neurotransmitter release at axonal terminals (Gu and Barry, 2011). Each Kv channel complex contains four voltage-sensing and pore-forming α subunits. Each α subunit consists of six membrane-spanning segments, and intracellular N- and C-terminal domains. Conserved N-terminal T1 domains form tetramers within a Kv channel subfamily, which is responsible for the proper assembly of a channel tetrameric complex (Li et al., 1992; Xu et al., 1995; Jan and Jan, 1997; Bixby et al., 1999; Choe, 2002; Jahng et al., 2002; Long et al., 2005). Kv3.1 channel, involved in fast spiking (Rudy et al., 1999; Kaczmarek et al., 2005; Bean, 2007), is the first identified ion channel that directly binds to KIF5 (Xu et al., 2010; Barry and Gu, 2012).

In this study, the observation that endogenous KIF5 often clusters along neurites prompted us to examine how Kv3 channels may regulate KIF5 function. Using a combination of approaches including protein biochemistry, live-cell imaging

Journal of Cell Science

assays, and Kv3.1 knockout mice, we have provided compelling evidence that the high-affinity multimeric binding between Kv3.1 T1 and KIF5B tail leads to KIF5 activation in clusters. Our results indicate that a Kv3.1-containing and anterogradely-moving punctum can astonishingly recruit up to 200 KIF5B-YFP motor dimers.

Results

Distribution pattern of endogenous KIF5 motors in neurons

In cultured hippocampal neurons, endogenous KIF5 motors are distributed smoothly and sometimes form clusters along neurites. Endogenous KIF5 clusters can be observed from both young neurons at 3 DIV (days *in vitro*) and older neurons at 21 DIV. KIF5B was concentrated in the soma, distributed rather smoothly along distal axons, and clustered in axonal endings. These clusters were not only at axonal growth cones, but also along axons. In a low-density neuron culture at 10 DIV, KIF5B clustered in many axonal growth cones, colocalizing with F-actin labeled with phalloidin (Fig. 1A). KIF5B was also distributed relatively more smoothly along the distal axon at a lower level (Fig. 1A). However, clusters with different sizes along axonal trunks were also present and they did not colocalize with F-actin, nor with tubulin clusters (Fig. 1B,C). If these clusters were moving carrier vesicles, they most likely contained many KIF5 motors, maybe tens or hundreds of KIF5 molecules, arguing against the current notion that each carrier vesicle contains only a few motors.

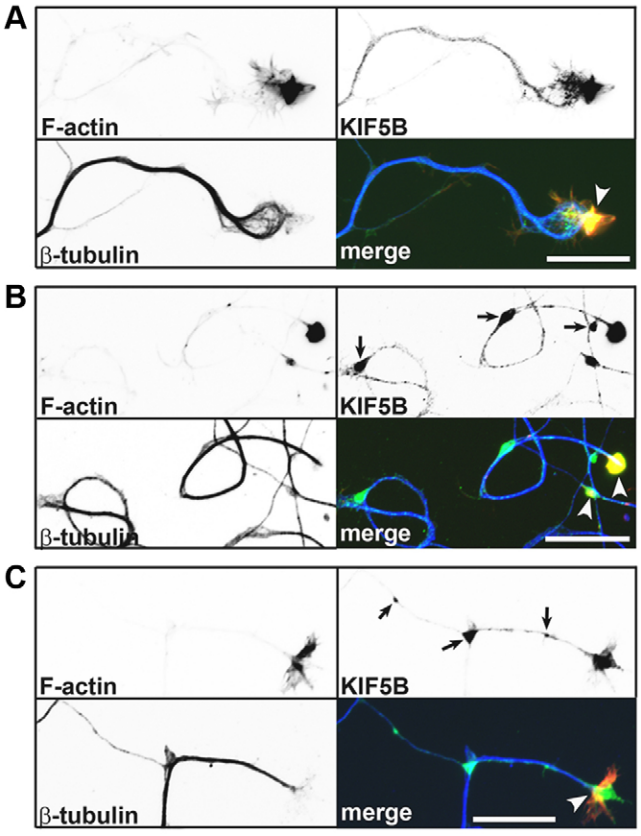

Fig. 1. Clustering of endogenous KIF5 motors in cultured hippocampal neurons. The low-density culture of hippocampal neurons from rat embryos (at E18) was used here at 10 DIV. (**A**) Endogenous KIF5B motors cluster (arrowhead) at the axonal growth cone. F-actin was labeled with phalloidin Alexa Fluor 546 (red in merged). KIF5B was stained with a rabbit anti-KIF5B antibody (green in merged) and β-tubulin was labeled with a mouse anti-β-tubulin antibody (blue in merged). Signals are inverted in single-channel images. (**B**,**C**) Clusters of KIF5B along axons with (indicated by white arrowheads) and without colocalizing F-actin (indicated by black arrows). Scale bars: 10 μm.

To understand the mechanism underlying KIF5 clustering, we wondered whether KIF5-binding proteins are involved. Mammalian KIF5 (KIF5A, KIF5B and KIF5C) contains an N-terminal motor domain for walking on microtubules, a stalk domain responsible for dimerization through coiled-coil regions, and a C-terminal tail domain for cargo binding. Among all the proteins known to bind to the KIF5 tail domain, Kv3 channel is the only one that forms functional tetramers (Xu et al., 2010). However, it remains unknown how strong the binding is, how many KIF5 tails one T1 tetramer can bind to, and what are the structural elements in KIF5 tail critical for the binding.

High-affinity and multimeric binding between the Kv3.1 T1 and KIF5B tail domains

To identify critical residues in the Kv3.1 T1-binding site within KIF5B tail, we made a series of GST-fusion proteins (Fig. 2A). Purified GST-T70 (a.a. 865–934) efficiently pulled down His-31T1 from bacterial lysates (Fig. 2B–E). Both the N-terminal (GST-Tail$_{865–896}$) and C-terminal (GST-Tail$_{892–934}$) portion of T70 also pulled down His-31T1, but less efficiently (Fig. 2B–D). The two share three basic residues ($R^{892}K^{893}R^{894}$) and have a net positive charge (>+5). Further shortening of the two regions from either ends eliminated the binding. GST-Tail$_{870–896}$, GST-Tail$_{865–891}$, GST-Tail$_{865–886}$, GST-Tail$_{875–896}$, GST-Tail$_{892–912}$, GST-Tail$_{913–934}$, GST-Tail$_{897–934}$, and GST-Tail$_{902–934}$, all failed to pull down His-31T1 (Fig. 2B–E). Whereas GST-Tail$_{875–919}$, missing 25 residues from both ends of T70, still pulled down His-31T1, GST-T70$_{RKR}$, with the three basic residues mutated to three acidic ones (Ds), completely lost the binding to His-31T1 (Fig. 2E).

We further performed the pulldown assay with purified proteins, showing GST-Tail and GST-T70, but not GST-T70$_{RKR}$, precipitated His-31T1 revealed by Colloidal blue staining (Fig. 3A). Surprisingly, smaller fragments, GST-Tail$_{892–934}$ and GST-Tail$_{865–896}$, did not clearly pull down purified His-31T1 (Fig. 3A), which most likely resulted from lower binding affinity and different sensitivity of Colloidal Blue staining and western blotting.

To determine the binding affinity between GST-T70 and His-31T1, we performed the Surface Plasmon Resonance (SPR) experiment with purified His-31T1 and four GST fusion proteins, GST, GST-T70, GST-Tail$_{892–934}$, and GST-T70$_{RKR}$. GST fusion proteins were immobilized on the sensor chip, while His-31T1 flowed over the chip surface in a binding buffer. His-31T1 bound to GST-T70 in high affinity (K_d: $6.0\pm1.4\times10^{-8}$ M; $n=4$) with fast association (K_{on}: $2.7\pm0.8\times10^{4}$ M; $n=4$) and relatively slow disassociation (K_{off}: $1.6\pm0.1\times10^{-3}$ M; $n=4$) (Fig. 3B, left). In contrast, GST-Tail$_{892–934}$ had nearly a thousand-fold reduction in binding affinity (K_d: $3.1\pm0.4\times10^{-5}$ M; $n=3$) (Fig. 3B, middle). The point mutant GST-T70$_{RKR}$ completely lost the binding to His-31T1 (Fig. 3B, right). Similar binding affinity was obtained between His-31T1 and GST-Tail containing the whole KIF5B tail domain. However, it is important to note that this binding assay was performed with isolated domains of Kv3.1 and KIF5B rather

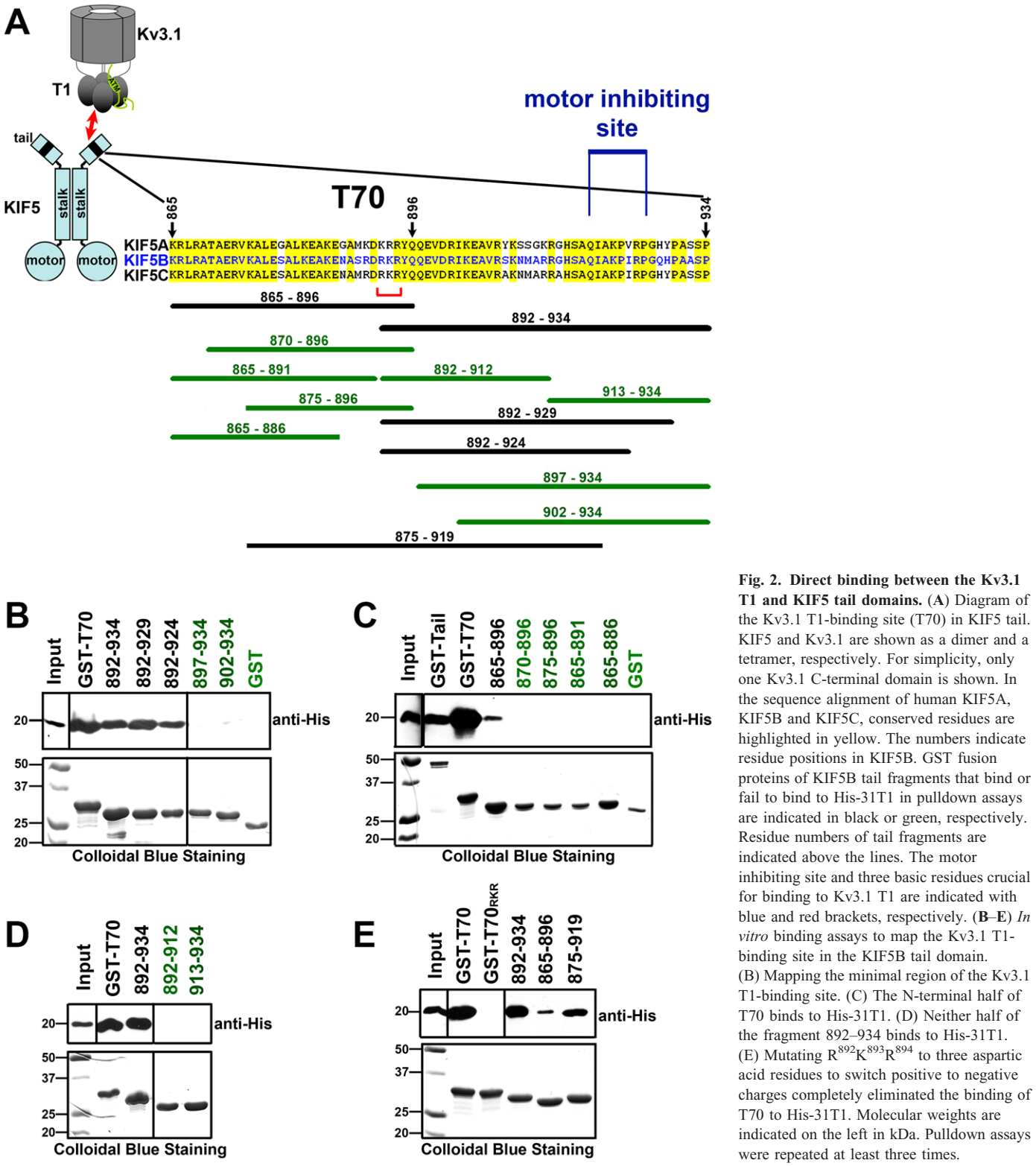

Fig. 2. Direct binding between the Kv3.1 T1 and KIF5 tail domains. (**A**) Diagram of the Kv3.1 T1-binding site (T70) in KIF5 tail. KIF5 and Kv3.1 are shown as a dimer and a tetramer, respectively. For simplicity, only one Kv3.1 C-terminal domain is shown. In the sequence alignment of human KIF5A, KIF5B and KIF5C, conserved residues are highlighted in yellow. The numbers indicate residue positions in KIF5B. GST fusion proteins of KIF5B tail fragments that bind or fail to bind to His-31T1 in pulldown assays are indicated in black or green, respectively. Residue numbers of tail fragments are indicated above the lines. The motor inhibiting site and three basic residues crucial for binding to Kv3.1 T1 are indicated with blue and red brackets, respectively. (**B**–**E**) *In vitro* binding assays to map the Kv3.1 T1-binding site in the KIF5B tail domain. (B) Mapping the minimal region of the Kv3.1 T1-binding site. (C) The N-terminal half of T70 binds to His-31T1. (D) Neither half of the fragment 892–934 binds to His-31T1. (E) Mutating $R^{892}K^{893}R^{894}$ to three aspartic acid residues to switch positive to negative charges completely eliminated the binding of T70 to His-31T1. Molecular weights are indicated on the left in kDa. Pulldown assays were repeated at least three times.

than the full-length proteins. Full-length Kv3.1 and KIF5B may have a different binding scenario due to the Kv3.1 T1 domains being fixed in a much more rigid position in the context of the whole-channel complex. Nonetheless, the SPR experiment confirmed the direct binding between Kv3.1 T1 and KIF5B tail, the critical role of the three basic residues and hence the role of electrostatic interaction, and provided the first value of the binding affinity between an ion channel and a kinesin motor.

To estimate how many KIF5B tails bind to one Kv3.1 T1 tetramer, we performed a pulldown assay with purified His-31T1 (~20 kDa) and GST-T70 (~32 kDa) in eight different molar ratios from 0:1 to 100:1. In precipitants, the amount of GST-T70

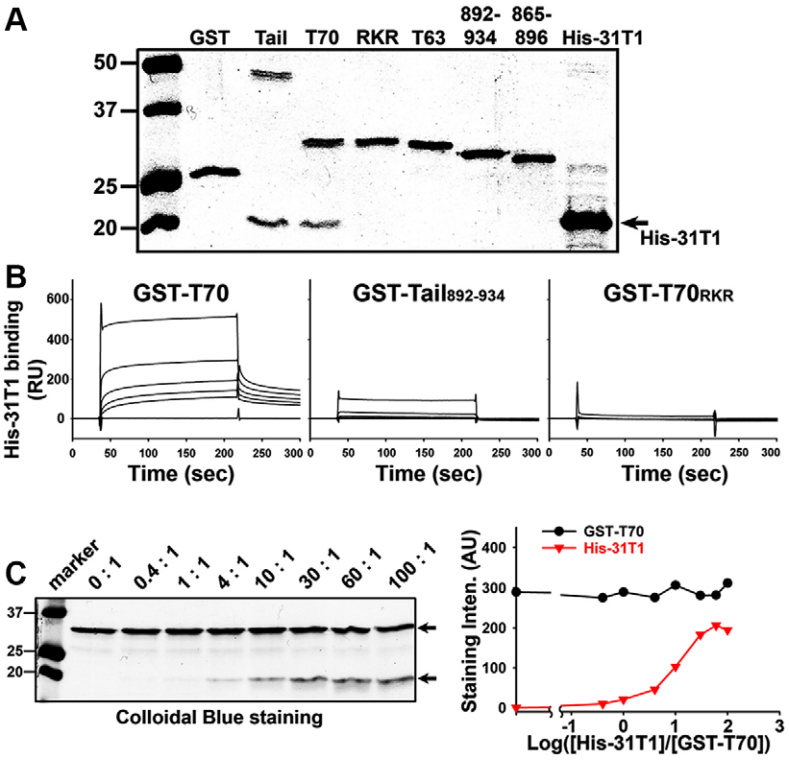

Fig. 3. Binding affinity and stoichiometry of Kv3.1 T1 and KIF5B tail domains. (**A**) Purified GST-Tail and GST-T70, but not GST-T70$_{RKR}$ pulled down purified His-31T1, indicated by the Colloidal Blue staining. Molecular weights (in kDa) are indicated on the left. (**B**) Binding response traces of His-31T1 to immobilized GST-T70 (left), GST-Tail$_{892–934}$ (middle) and GST-T70$_{RKR}$ (right), in the SPR experiment. Solutions containing six different concentrations (0, 200 nM, 600 nM, 2 μM, 10 μM and 100 μM) of His-31T1 were flowed over the chip. The spikes in the traces at the highest concentration of His-31T1 are most probably due to buffer change. Triton X-100 (0.1%) was included in the stock buffer of high-concentration purified proteins to increase the solubility, but not in the binding buffer used in SPR. (**C**) Estimation of the stoichiometry of the Kv3.1 T1 and KIF5B tail binding complex. In the left panel, purified GST-T70 (3.2 μg) was first coated on glutathione beads (30 μl total volume; 100% binding assumed), which were further incubated with different amounts of purified His-31T1. The molar ratios between His-31T1 (~20 kDa) and GST-T70 (~32 kDa) were 0:1, 0.4:1, 1:1, 4:1, 10:1, 30:1, 60:1, 100:1. The right panel shows the staining intensity graph of GST-T70 (black circles) and His-31T1 (red triangles). The protein gel was scanned as a TIFF image file and the intensity of protein bands were measured and subtracted with the background value.

stayed constant, whereas the amount of His-31T1 increased and saturated at an intensity ratio of 200:320 (AU) (His-31T1:GST-T70) (Fig. 3C), suggesting that the stoichiometry of the binding complex is ~1:1. Since the T1 domain is highly conserved within the Kv3 channel subfamily, one Kv3 channel tetramer complex, including both homotetramers and heterotetramers, can bind up to four KIF5B motors (or four heavy chain dimers).

Kv3.1 T1 competes with the KIF5B motor domain and microtubules but not with KLC1 for binding to KIF5B tail

KIF5 C-terminal tail domains contain overlapping binding sites for cargo recognition, auto-inhibition, and for interactions with myosin and microtubules (Twelvetrees et al., 2010; Wong and Rice, 2010; Xu et al., 2010; Andrews et al., 1993; Diefenbach et al., 1998; Coy et al., 1999; Friedman and Vale, 1999; Huang et al., 1999; Hackney and Stock, 2000; Setou et al., 2002; Cai et al., 2005; Glater et al., 2006) (Fig. 4A). To determine how these proteins and Kv3.1 T1 affect each other's binding to KIF5B tail, we performed competitive *in vitro* binding assays, with a constant amount of GST-Tail, and two different His-tagged proteins in different molar ratios. Increasing amounts of His-31T1 did not decrease the binding between GST-Tail and His-KLC1 (Fig. 4B,C; supplementary material Fig. S1A,B), suggesting Kv3.1 T1 does not compete with KLC1 for binding to KIF5B tail. In contrast, His-Motor did compete with His-31T1 for binding to KIF5B tail, although the binding between GST-Tail and His-Motor appeared weaker (Fig. 4D; supplementary material Fig. S1C).

By using microtubule *in vitro* assembly and pulldown assays, we further examined the role of Kv3.1 T1 in the KIF5B tail and microtubule binding. GST-Tail and GST-T70, but not GST, GST-T63 (a.a. 758–820, containing the KLC1 binding site), or GST-T70$_{RKR}$, bound to microtubules (Fig. 4E,F; supplementary material Fig. S1D,E). Interestingly, His-31T1 effectively competed GST-T70 away from microtubules (the P fraction) in a concentration-dependent manner (Fig. 4G; supplementary material Fig. S1F). His-31T1 does not bind to microtubules, since even in high concentration His-31T1 did not show up in the pellet fraction of microtubules (Fig. 4G; supplementary material Fig. S1F). Therefore, Kv3.1 channels likely activate KIF5B motor activity by releasing the tail binding to both the motor domain and microtubules.

Binding proteins of KIF5 differentially affect the localization of KIF5 tail fragments

To evaluate these *in vitro* results obtained with protein biochemical assays, we designed a series of experiments in neurons. We determined the roles of four known KIF5-binding proteins in regulating KIF5 distribution and motility as comparison. First, we examined the colocalization between KIF5 motor and these four proteins in neurons. Among cultured hippocampal neurons at 21 DIV, some expressed Kv3.1b, which colocalized with KIF5 in clusters (Fig. 5A, top) (Xu et al., 2010). KLC1 extensively colocalized with KIF5 including clusters (Fig. 5A, 2nd row). Whereas the KIF5-tail-binding SNAP25 partially colocalized with KIF5 in clusters, VAMP2, a cargo of KIF5, colocalized with KIF5 significantly less and no clear colocalization in clusters was observed (Fig. 5A, 3rd and 4th rows). Therefore, the immunostaining results show that different KIF5-binding proteins colocalize with KIF5 in different patterns.

Next, to understand how these proteins bind to KIF5 tail in living neurons, we examined their effects on KIF5B tail distribution using coexpression. The KIF5 tail domains contain binding sites for binding cargos, and are commonly used as dominant-negative constructs to disrupt endogenous KIF5

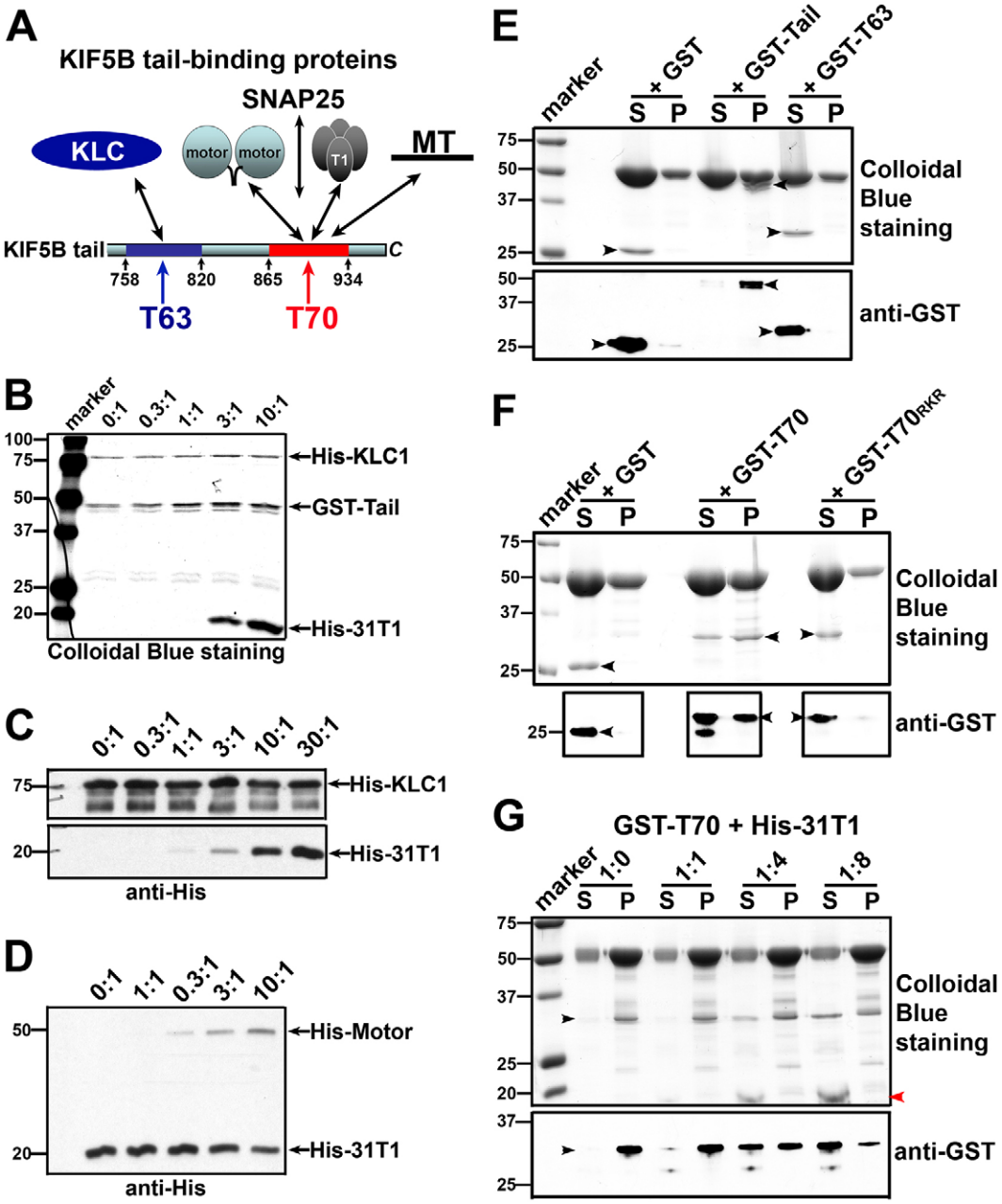

Fig. 4. Kv3.1 T1 competes with microtubules but not KLC1 for binding to KIF5B tail. (**A**) Diagram of the KIF5B tail domain and five of its binding proteins. The KLC-binding site (T63) is located between residues 758 and 820, highlighted in blue. The Kv3 T1-binding site (T70) is between residues 865 and 934, highlighted in red, which overlaps with binding sites for KIF5 motor domain, microtubules and SNAP25. (**B**) His-31T1 did not compete with His-KLC1 for binding to GST-Tail. GST-Tail (3.5 µg) was first coated on glutathione beads and further used to pull down purified His-KLC1 (5.6 µg, so that GST-Tail and His-KLC1 are in a 1:1 molar ratio) mixed with different amounts of His-31T1. Molar ratios between His-31T1 and His-KLC1 used were 0:1, 0.3:1, 1:1, 3:1 and 10:1. (**C**) Western blotting with an anti-6×His antibody in an experiment similar to B, except that a lower amount of GST-Tail (2.5 µg), an additional condition (30:1) and 10% loading compared to protein gels were used. (**D**) Increased amount of His-Motor reduced the amount of His-31T1 binding to GST-Tail. (**E,F**) Purified GST-Tail and GST-T70, but not GST, GST-T63 or GST-T70$_{RKR}$, bound to microtubules. Microtubules were assembled *in vitro* with purified tubulins for 20 minutes, then incubated with purified GST fusion proteins (around 5 µg total) for another 30 minutes and pelleted with a high-speed spin. Pellets were resolved with sample buffer equal to the supernatant in volume, and equal volume of supernatants and dissolved pellets were loaded on a SDS-PAGE gel. Protein bands were stained with Colloidal Blue (top). GST fusion proteins were further revealed with western blotting using an anti-GST antibody (10% loading) (bottom). (**G**) Purified GST-T70 and His-31T1 were mixed in four different molar ratios, 1:0, 1:1, 1:4 and 1:8. In this experiment, microtubules were assembled in the presence of 100 µM paclitaxel to further stabilize assembled microtubules. The supernatants and pellets were resolved in SDS-PAGE and revealed by both Colloidal Blue staining (top) and western blotting (10% loading) using an anti-GST antibody (bottom). Since there was no washing step after assembled microtubules were pelleted, very faint bands in the pellet lane are due to supernatant contamination, even when the protein does not bind to microtubules. All *in vitro* binding experiments were repeated at least three times. Molecular weights are indicated on the left in kDa. S, supernatant; P, pellet; black arrowheads, GST fusion proteins; red arrowheads, His-31T1.

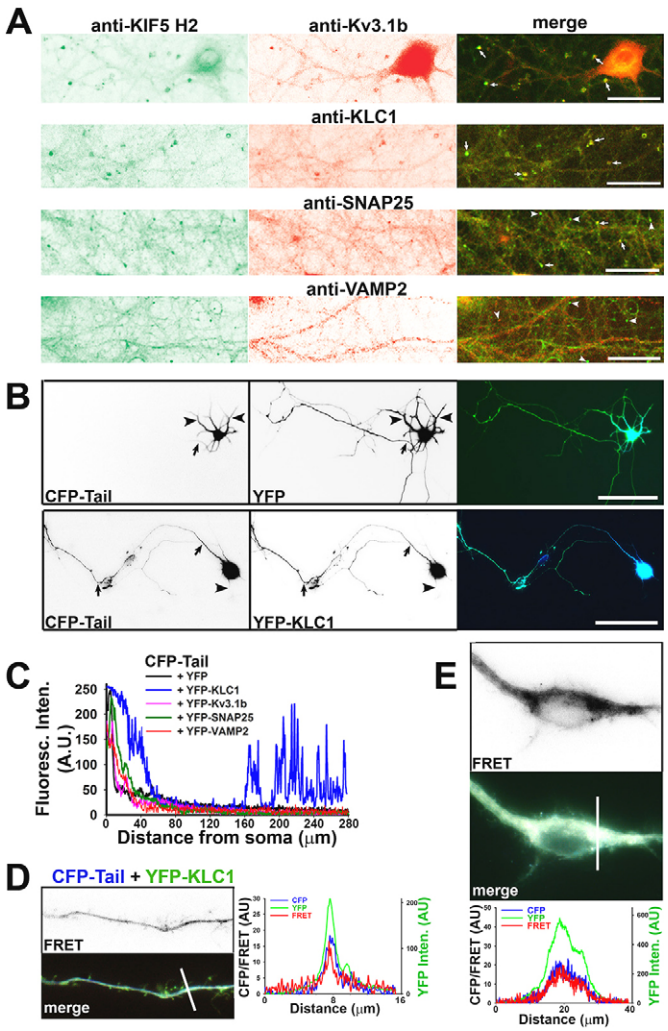

Fig. 5. KIF5-binding proteins differentially regulate KIF5B tail localization. (**A**) Co-staining of cultured hippocampal neurons at 20 DIV for endogenous KIF5 (mouse H2 antibody in green) and its binding proteins (Kv3.1b, KLC1, SNAP25 and VAMP2; in red). White arrows, colocalizing puncta; white arrowheads, non-colocalizing puncta. (**B**) CFP-Tail was restricted in somatodendritic regions in 8-DIV neurons expressing CFP-Tail and YFP (top). Coexpression of YFP-KLC1 (green in merged) brought CFP-Tail (blue in merged) into distal axons (bottom). Black arrows, axons; black arrowheads, dendrites. (**C**) CFP-Tail intensity profiles along axons in the presence of various YFP fusion proteins. Only the expression of YFP-KLC1, but not YFP-Kv3.1b, YFP-SNAP25 nor YFP-VAMP2, targeted CFP-Tail into distal axons. (**D**) Strong FRET signals (inverted in single channel and red in merged) were detected along axons between CFP-Tail (blue) and YFP-KLC (green); 17 out of 19 neurons had strong FRET signals. (**E**) Strong FRET signals were also detected in the soma of transfected neurons. Scale bars: 25 μm (A); 80 μm (B).

function (Bi et al., 1997; Cross and Scholey, 1999; Setou et al., 2002; Konishi and Setou, 2009). YFP-Tail was mainly concentrated in the somatodendritic regions when expressed alone in cultured hippocampal neurons, whereas YFP-KLC1 was present in both axons and dendrites. When coexpressed, YFP-KLC1, but not YFP, brought CFP-Tail into distal axons (Fig. 5B). In fact, YFP-Kv3.1b, YFP-SNAP25 and YFP-VAMP2, all failed to bring CFP-Tail into distal axons (Fig. 5C), although all four YFP constructs were present in both dendrites and axons in transfected neurons. Whereas the tail-microtubule binding is disrupted by KLC (Wong and Rice, 2010) and Kv3 T1 domain (Fig. 4G), only coexpression of YFP-KLC1 but not YFP-Kv3.1b brought CFP-Tail into distal axons, suggesting binding to microtubules may not be the only mechanism to trap the tail domain in somatodendritic regions.

Using fluorescence resonance energy transfer (FRET) imaging, we examined the physical interaction between KIF5B tail and KLC1 in living neurons. CFP-Tail and YFP-KLC1 were highly colocalized and yielded strong FRET signals in both distal axons and soma (Fig. 5D,E). Consistent with the results of binding assays (Fig. 3A), CFP-KLC1 and YFP-T63, but not CFP-KLC1 and YFP-T70, yield strong FRET signals in both distal axons and soma (supplementary material Fig. S2). Furthermore, when coexpressed in hippocampal neurons, YFP-T70 but not YFP-$T70_{RKR}$ significantly reduced the axonal level of Kv3.1bHA (supplementary material Fig. S3A,B). Using FRET imaging, we found that YFP-T70 and CFP-Kv3.1b, but not YFP-$T70_{RKR}$ and CFP-Kv3.1b, had significant FRET signals in neuronal soma (supplementary material Fig. S3C,D). Therefore, these results obtained using living neurons are consistent with the biochemical data. Importantly, these results have identified two smaller regions within KIF5B tail, which can be used as dominant-negative constructs to disrupt the transport of different groups of cargos, for instance, KLC-dependent and -independent groups.

Opposite effects of the binding of Kv3.1 and KLC1 on KIF5B distribution

How various binding proteins to the KIF5 tail domain affect KIF5 activity and potentially cluster the motor remains unknown. When expressed in neurons, the distribution pattern of KIF5B-YFP was similar to that of endogenous KIF5. KIF5B-YFP was more uniformly concentrated in distal axons (Fig. 6A, top), although clusters, especially at the axonal endings and sometimes along axonal trunks, were observed. Surprisingly, mutating the three basic residues ($R^{892}K^{893}R^{894}$) in the KIF5B tail domain to three Ds completely changed its distribution pattern. $KIF5B_{RKR}$-YFP exclusively formed clusters in various sizes in axonal endings and along axons (Fig. 6A, bottom). It was difficult to find the soma and dendrites of the neuron expressing $KIF5B_{RKR}$-YFP. This is a more pronounced clustered pattern than that of the tailless KIF5B (Xu et al., 2010). The mutation eliminated the binding of microtubules to KIF5 tail, which should be at least partially responsible for the effect.

Using cotransfection, we examined the effects of four different KIF5-binding proteins on the distribution patterns of KIF5B-YFP and $KIF5B_{RKR}$-YFP. In the presence of coexpressed CFP-KLC1, KIF5B-YFP distribution pattern remained unchanged. In sharp contrast, in the presence of coexpressed CFP-Kv3.1b, KIF5B-YFP formed clusters in various sizes along axons (Fig. 6B,D,E). Interestingly, coexpressed CFP-KLC1 completely converted $KIF5B_{RKR}$-YFP from a highly clustered pattern to a uniformed pattern similar to that of KIF5B-YFP, which may suggest an inhibitory role of KLC1 in KIF5 activation. In the presence of coexpressed CFP-Kv3.1b, $KIF5B_{RKR}$-YFP remained highly clustered (Fig. 6C–E). Only a very small fraction of the clusters contained CFP-Kv3.1b along axons (Fig. 6C, bottom), in which endogenous KIF5 may dimerize with the mutant to bind to Kv3.1. Thus, expression of Kv3.1 clusters KIF5B motors, whereas expression of KLC1 tends to disperse them (Fig. 6D,E). Different from CFP-KLC1 and CFP-Kv3.1b, both CFP-SNAP25

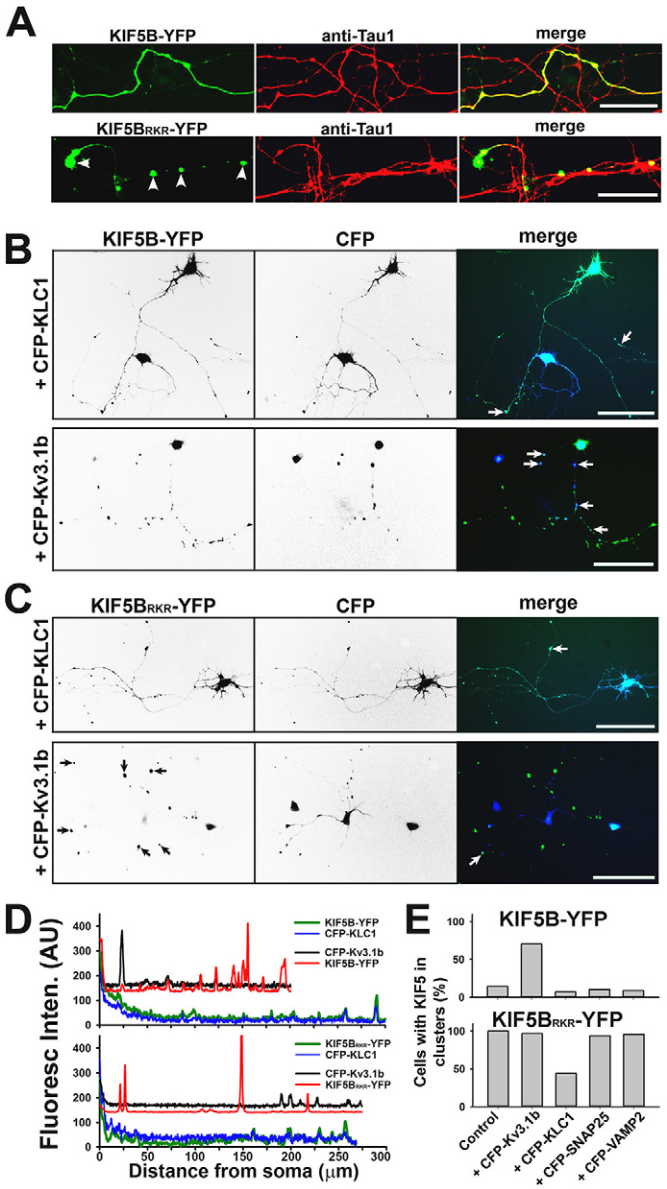

Fig. 6. Mutating the three charged residues or the presence of Kv3.1 clusters KIF5B-YFP. (**A**) Relatively smooth distribution of KIF5B-YFP (green) along axons of hippocampal neurons (top), which were transfected at 5 DIV, fixed and stained for axonal marker, Tau1 (red), two days later. Highly clustered pattern of $KIF5B_{RKR}$-YFP (green) along axons (labeled for Tau1 in red) (bottom). Arrowheads indicate clusters of $KIF5B_{RKR}$-YFP along the axon segment. (**B**) Distribution patterns of KIF5B-YFP (green in merged) when coexpressed with either CFP-KLC1 (top) or CFP-Kv3.1b (bottom) in hippocampal neurons. White arrows indicate colocalizaing clusters. (**C**) Distribution patterns of $KIF5B_{RKR}$-YFP (green in merged) when coexpressed with either CFP-KLC1 (top) or CFP-Kv3.1b (bottom) in hippocampal neurons. YFP is in green and CFP is in blue in merged images. Signals are inverted in single-channel images. White arrows, colocalizating clusters; black arrows, $KIF5B_{RKR}$-YFP clusters without CFP-Kv3.1b. (**D**) Profiles of fluorescence intensity along axons in B (top) and C (bottom). (**E**) Summary of the clustering effect of CFP-tagged KIF5-binding proteins on KIF5B-YFP (top) and $KIF5B_{RKR}$-YFP (bottom). Scale bars: 10 μm (A); 100 μm (B,C).

and CFP-VAMP2 partially colocalized with KIF5B-YFP and $KIF5B_{RKR}$-YFP, but did not change their distribution patterns (Fig. 6E).

Kv3.1b, but not other KIF5-binding proteins, markedly increases the moving frequency of KIF5B-YFP anterograde puncta

To further examine how these binding proteins affect KIF5B motor motility, we performed live cell imaging in high magnification on cultured hippocampal neurons transfected with KIF5B-YFP. When expressed alone, moving puncta of KIF5B-YFP were only occasionally observed (Fig. 7A,G; supplementary material Movie 1). In the present study, we only quantified detectable KIF5B-YFP puncta, but not moving vesicles with only one or a few KIF5B-YFP. In the presence of CFP-Kv3.1b, but not CFP-KLC1, CFP-SNAP25 or CFP-VAMP2, the frequency of moving puncta containing KIF5B-YFP markedly increased (Fig. 7B,C,G; supplementary material Movies 2, 3). There was no clear increase in velocity. Therefore, among the four KIF5-binding proteins examined, CFP-Kv3.1b is the only one that can activate and cluster KIF5B-YFP.

In sharp contrast to KIF5B-YFP, more than half of $KIF5B_{RKR}$-YFP puncta were moving (Fig. 7D,G,H; supplementary material Movie 4). The increased moving frequency for $KIF5B_{RKR}$-YFP puncta was mainly in the anterograde direction (Fig. 7H). Coexpression of CFP-Kv3.1b, CFP-SNAP25 or CFP-VAMP2 did not affect the frequency of moving puncta of $KIF5B_{RKR}$-YFP (Fig. 7E,H; supplementary material Movie 5), whereas coexpression of CFP-KLC1 significantly reduced the frequency (Fig. 7F,H; supplementary material Movie 6). Thus, Kv3.1 and KLC1 differ in regulating KIF5B motor motility. Importantly, our imaging results showed that many clusters of $KIF5B_{RKR}$-YFP or the wild type in the presence of CFP-Kv3.1b were actually mobile, and most of them were in the anterograde direction.

Kv3.1 significantly increases the copy number of KIF5B-YFP on carrier vesicles

Because of the strong fluorescence intensity of these moving puncta, we suspected that they might contain many YFP molecules. We previously reported the measurement of YFP-Kv1.2 in axonal transporting puncta using quantitative microscopy calibrated with yeast strains expressing various YFP-fusion proteins (Gu and Gu, 2010; Wu and Pollard, 2005). Using the same strategy, we first measured the fluorescence intensities in anterograde moving puncta containing either KIF5B-YFP or $KIF5B_{RKR}$-YFP, in the absence or presence of CFP-Kv3.1b or CFP-KLC1 (Fig. 8A,B). Fluorescence intensities of retrograde moving and stationary puncta were also measured. Next, we calculated the numbers of KIF5B dimers with previously calibrated standards (Gu and Gu, 2010). In the presence of CFP-Kv3.1b, the estimated number of KIF5B-YFP dimers markedly increased for anterograde (KIF5B-YFP alone: 29.2±4.2; + CFP-Kv3.1b: 187.8±47.3), retrograde (KIF5B-YFP alone: 27.8±4.9; + CFP-Kv3.1b: 327.3±96.1), or stationary puncta (KIF5B-YFP alone: 76.4±9.5; + CFP-Kv3.1b: 764.8±106.1) (Fig. 8C). $KIF5B_{RKR}$-YFP dimer numbers in various puncta markedly increased compared to KIF5B-YFP and the coexpression of CFP-Kv3.1b did not further increase those numbers ($KIF5B_{RKR}$-YFP alone anterograde: 161.3±45.8; + CFP-Kv3.1b anterograde: 167.2±45.8) (Fig. 8C). Coexpression of CFP-KLC1 also increased the number of KIF5B-YFP (anterograde: 86.8±21.8), but significantly decreased the number of $KIF5B_{RKR}$-YFP (anterograde: 84.7±15.5), especially in anterograde moving puncta (Fig. 8C). Coexpression of CFP-SNAP25 and CFP-VAMP2 had no clear effect on the content of KIF5B-YFP

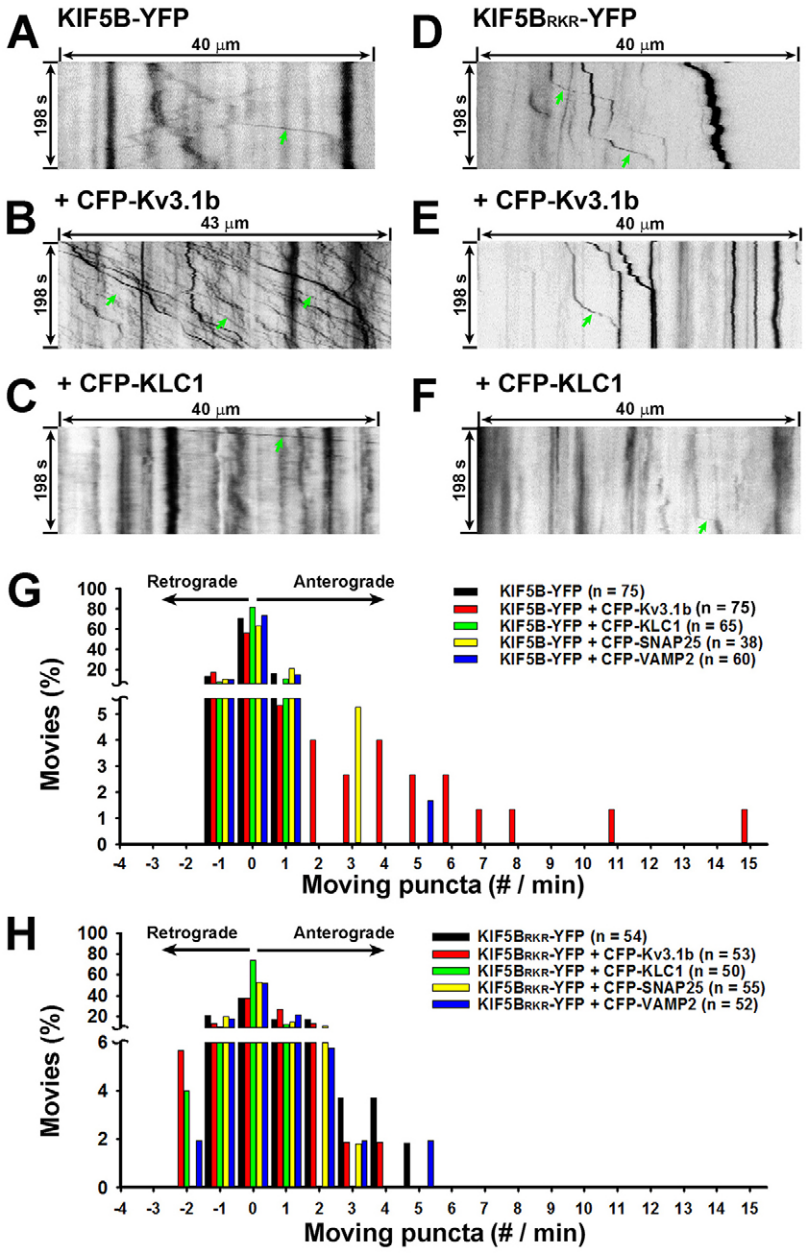

Fig. 7. CFP-Kv3.1b, but not CFP-KLC1, CFP-SNAP25 and CFP-VAMP2, increased the mobility of KIF5B-YFP puncta. (**A**) Kymograph of anterograde transport of KIF5B-YFP puncta along an axonal segment. (**B**) Kymograph of anterograde transport of KIF5B-YFP puncta along an axonal segment in the presence of CFP-Kv3.1b. (**C**) Kymograph of anterograde transport of KIF5B-YFP puncta along an axonal segment in the presence of CFP-KLC1. (**D**) Kymograph of anterograde transport of $KIF5B_{RKR}$-YFP puncta along an axonal segment. (**E**) Kymograph of anterograde transport of $KIF5B_{RKR}$-YFP puncta along an axonal segment in the presence of CFP-Kv3.1b. (**F**) Kymograph of anterograde transport of $KIF5B_{RKR}$-YFP puncta in the presence of CFP-KLC1. Green arrows indicate anterograde-moving puncta. (**G**) Frequency of axonal transport of KIF5B-YFP puncta in the presence of CFP-Kv3.1b (red), CFP-KLC1 (green), CFP-SNAP25 (yellow), CFP-VAMP2 (blue) or alone (black). (**H**) Frequency of axonal transport of $KIF5B_{RKR}$-YFP puncta in the presence of CFP-tagged proteins. The movie number is given as 'n', which shows the number of movies for each condition. Statistical results were obtained from at least five independent transfections.

moving puncta. Therefore, our results indicate that Kv3 channels can cluster KIF5 motors during intracellular transport. This has raised an intriguing question. Can deletion of Kv3.1 channels influence the clusters of KIF5 motors *in vivo*?

KIF5 clusters in cerebellar neurons from Kv3.1 knockout mice are reduced

We examined the KIF5B distribution pattern in Kv3.1 KO mice, which were published previously (Ho et al., 1997; Sánchez et al., 2000; Hurlock et al., 2009). The KO mice were confirmed with western blotting and PCR-based genotyping (Fig. 9A,B). In the western blotting of mouse brain lysates, the expression of Kv3.1b was completely eliminated, but the expression of KIF5 and its binding proteins, including KLC1, GRIP1 and SNAP25, remained unchanged (Fig. 9A). Kv3 channels are highly expressed in mouse cerebellum. In particular, Kv3.1 channels are expressed in cerebellar granule cells (Weiser et al., 1994; Grigg et al., 2000; Rudy and McBain, 2001). Therefore, Kv3.1b is present in the parallel fibers (axons from granule cells) in the molecular layer, but does not express in Purkinje neurons (Puente et al., 2010). In coronal sections of cerebellum, Kv3.1b and KIF5B were present and colocalized in both molecular layer and granule cell layer (Fig. 9C). In Kv3.1 KO mice, Kv3.1b staining markedly reduced, close to background (Fig. 9D). Whereas the overall level of KIF5B remained the same in the KO mice, its KIF5B clusters significantly reduced (WT: 3017±137; $Kv3.1^{-/-}$: 2545±121; P=0.016) (Fig. 9E,F). In brain sections, it is difficult to determine where the clusters come from, axons, dendrites, soma or even non-neuronal cells.

To clearly visualize KIF5 clusters along individual axons, we performed cerebellar neuron culture, using the similar condition with the hippocampal neuron culture, which favors the survival

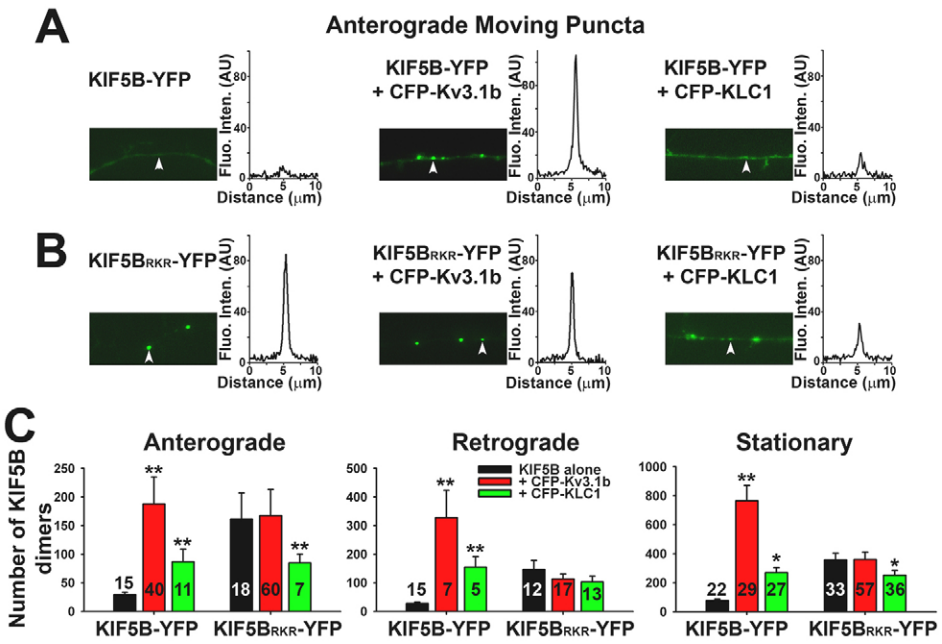

Fig. 8. Tetrameric Kv3 channels markedly increase the KIF5B-YFP number in a carrier vesicle. (**A**) Quantification of the YFP fluorescence of anterogradely moving puncta containing KIF5B-YFP along an axonal segment either alone (left) or in the presence of CFP-Kv3.1b (middle) or CFP-KLC1 (right). The image of axonal segment is on the left and the intensity profile along a 10-μm line crossing the axon is on the right. White arrowheads indicate anterogradely moving puncta. (**B**) Quantification of the YFP fluorescence of anterogradely moving puncta containing $KIF5B_{RKR}$-YFP along an axonal segment either alone (left), or in the presence of CFP-Kv3.1b (middle) or CFP-KLC1 (right). White arrowheads indicate anterogradely moving puncta. (**C**) Summary of estimated numbers of KIF5B-YFP dimers or $KIF5B_{RKR}$-YFP dimers in various puncta under different coexpression conditions. One-way ANOVA followed by Dunn's test, $^{**}P<0.01$; $^{*}P<0.05$; number of experiments is indicated for each bar.

of granule cells. Kv3.1 and Kv3.3 are expressed in cerebellar granule cells (Grigg et al., 2000; Rudy and McBain, 2001; Weiser et al., 1994). These neurons were clearly smaller than hippocampal neurons at the same developmental stage, but generated action potentials at markedly higher frequency (Fig. 10A, top). Around 3 weeks in culture, WT cerebellar neurons, but not Kv3.1 KO neurons, generated high frequency spiking up to 100 Hz (Fig. 10A). The after hyperpolarization of action potentials was clearly reduced in the KO neurons (Fig. 10B), consistent with Kv3.1 deletion. The input–output curves were clearly different for the WT and KO neurons around 3 weeks, but not before 2 weeks (Fig. 10C). In WT neurons, endogenous KIF5 formed clusters along neurites colocalizing with KLC1 (Fig. 10D,F). In KO neurons, KIF5 clusters were still present, although there was clear reduction of clusters (Fig. 10E,G). Using the same quantification method in Fig. 9E, we found that KIF5B staining had a clear clustered pattern along WT axons, and became much smoother along Kv3.1 KO axons (Fig. 10H,I). Therefore, the results from cerebellum sections and cultured neurons are consistent. However, it is important to note that despite clear reduction in the KO mice, KIF5B clusters were still present, suggesting multiple proteins and/or mechanisms may contribute to KIF5 clustering.

Discussion

In this study, we show that Kv3 channels activate KIF5 by relieving the two inhibitory mechanisms that are mediated by the tail-motor and tail-microtubule binding (supplementary material Fig. S4A). Kv3 tetramers cluster KIF5 motors via direct and multimeric high-affinity binding, and hence increase the number of KIF5 motors on the carrier vesicle (supplementary material Fig. S4B). To our knowledge, this is the first report on a mechanism underlying the regulation of the motor number on a carrier vesicle. Our study also indicates that different KIF5-binding proteins, even with overlapping binding sites, can ride the KIF5 motor in different ways, which is likely critical for the specificity of KIF5-mediated transport. Therefore, this study has provided novel mechanistic insights into the specificity of cargo transport and cargo-mediated regulation of kinesin motors.

The high-affinity and multimeric binding between Kv3 T1 and the KIF5 tail is a novel mechanism underlying KIF5 clustering

Kv3.1 is the first identified ion channel that directly binds to KIF5 (Xu et al., 2010). Among all the known proteins that physically interact with KIF5, Kv3 is the only one whose function relies on proper tetramerization and tetramerization is required for Kv3-KIF5 binding (Xu et al., 2010), raising an intriguing possibility that Kv3 channels may at least be partially responsible for KIF5 clustering, observed in endogenous KIF5 motors (Fig. 1). To better understand the biochemical basis of the interaction between Kv3 T1 and KIF5 tail, we first performed a systematical mutagenesis of the Kv3.1 T1-binding site (a 70-residue region) of KIF5B tail and identified three basic residues crucial for the binding (Fig. 2). Next, in the SPR experiment, we determined the binding affinity ($K_d=6.0\pm1.4\times10^{-8}$ M) between Kv3.1 T1 and its binding site within KIF5B (Fig. 3B), which provides the first quantification for the binding strength between an ion channel and a molecular motor. The K_d is within the binding range of a monoclonal antibody and its target, comparable to the binding affinity between KIF5 and GRIP1 ($K_d=1.9\times10^{-8}$ M) (Setou et al., 2002) and higher than the binding affinity between Sunday Driver/JIP3 and KIF5 ($K_d=1.8\times10^{-6}$ M) (Sun et al., 2011). Furthermore, our pulldown experiments suggest that a Kv3.1 channel tetramer can simultaneously bind up to four KIF5 heavy chains (Fig. 3C). The competition experiments show that purified His-31T1 competed with His-Motor and microtubules but not with His-KLC1, suggesting Kv3.1 may activate the KIF5B motor by relieving the inhibition of the motor domain and the microtubule binding to KIF5 tail (Fig. 4). These biochemical data have revealed critical information regarding how Kv3 channels may activate and cluster KIF5 motors. It is important to note that the interactions revealed with protein biochemical assays are subject

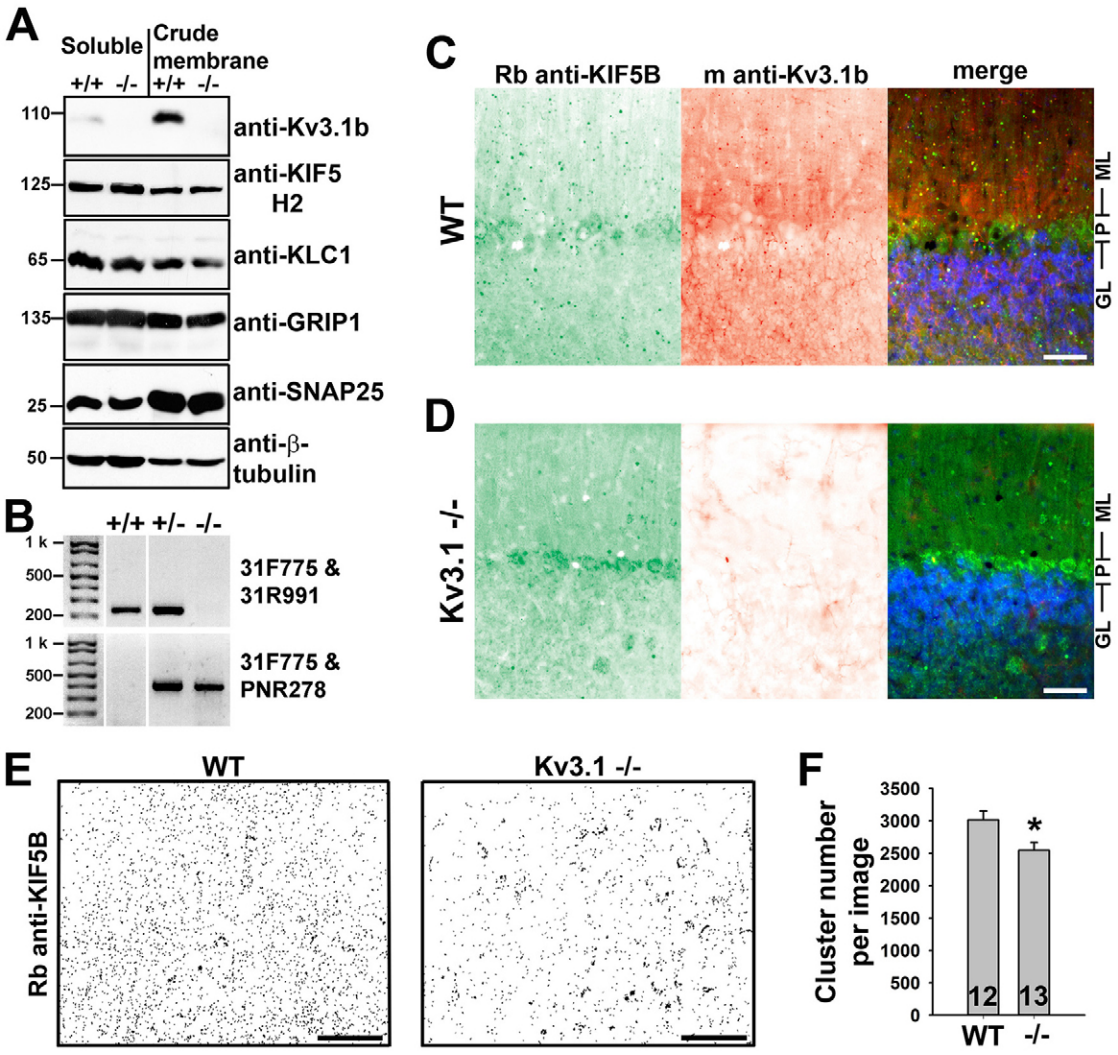

Fig. 9. KIF5 clusters reduced in cerebellar neurons of Kv3.1 knockout mice. (**A**) Expression of Kv3.1b, KIF5 and KIF5-binding proteins in brains of Kv3.1 knockout (−/−) and wild-type (+/+) mice. Soluble fractions (left) and crude membranes (right) are compared. Molecular weights (in kDa) are indicated on the left. (**B**) Genotyping of Kv3.1 heterozygotes (+/−), homozygotes (−/−), and wild-type mice. DNA ladders are on the left in bp. (**C,D**) Kv3.1b and KIF5B staining patterns in coronal sections of cerebellum from wild-type (C) and Kv3.1 KO (D) mice. P, Purkinje cell layer; GL, granule cell layer; ML, molecular layer. (**E**) To quantify the KIF5B clusters from the wild-type (left) and *Kv3.1*$^{-/-}$ (right) sections, images were thresholded and binarized to show pixel clusters. (**F**) Summary of the clusters per image (40× objective lens). The number of experiments is indicated within the bars;*$P<0.05$ (*t*-test). Scale bars: 300 μm (C,D); 100 μm (E).

to variety of regulations *in vivo*. Therefore, we have further carried out various experiments using living neurons.

Different cargos ride KIF5 motors differently, suggesting cargo-directed transport

Kv3.1 is unique among the KIF5-binding proteins examined in this study in regulating KIF5B function. Although KLC1 was also shown to release the tail-motor domain binding and tail-microtubule binding (Wong and Rice, 2010), Kv3.1 and KLC1 differ in multiple ways in regulating KIF5 motor activity. First, they bind to different regions in KIF5B tail (Fig. 4). Second, CFP-Kv3.1b but not CFP-KLC1 clustered KIF5B-YFP along axons (Fig. 6). Third, interestingly, CFP-KLC1 but not CFP-Kv3.1b dispersed the clustered pattern of $KIF5B_{RKR}$-YFP (Fig. 6). In Fig. 6, the changes of distribution patterns were very dramatic and clear. Fourth, they had different effects on KIF5B-YFP moving puncta (Fig. 7). KLC1 apparently did not compete with Kv3.1 channels for binding to KIF5 (Fig. 4E), nor clusters KIF5 (Fig. 6). In contrast to the sophisticated roles of KLC1 (Wong and Rice, 2010; Cai et al., 2007), the action of Kv3.1 appears to be straightforward, which is to activate and cluster KIF5B motors. We also examined two other KIF5-binding proteins, SNAP25 and VAMP2. Although they have overlapping binding sites with Kv3 in KIF5 tail, both failed to cluster or activate KIF5 motors (Fig. 6E and Fig. 7). Therefore, although the KIF5/kinesin-1 motor can be activated by other binding proteins, our study has clearly demonstrated that the Kv3 channels tetramers uniquely cluster KIF5 motor, contributing to the specificity of both cargo loading and cargo-regulated activation.

Regulation of the copy number of KIF5 motors on a transporting vesicle

This study has revealed a novel mechanism underlying the regulation of the copy number of KIF5B motors on a transporting

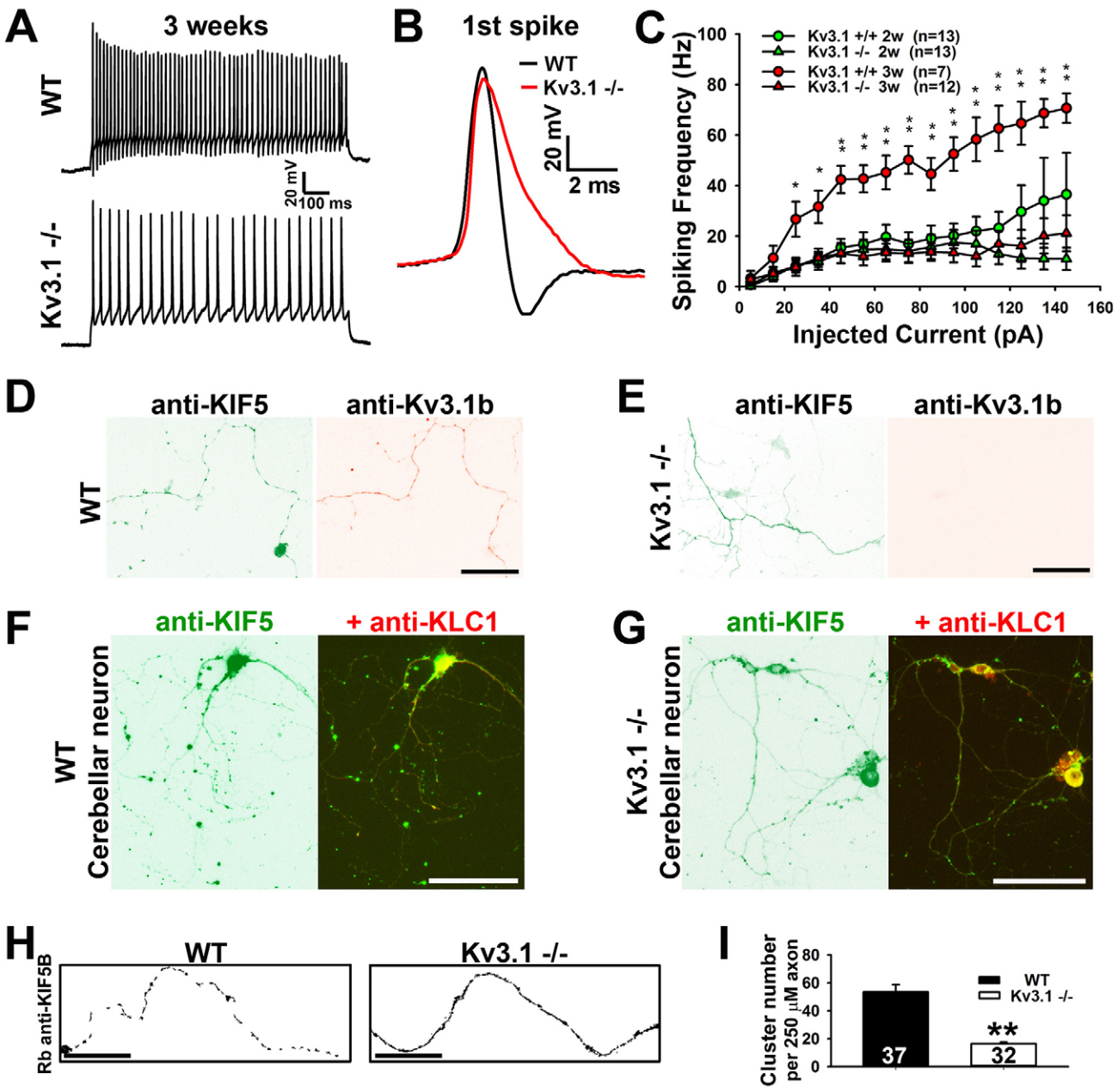

Fig. 10. Deletion of Kv3.1 reduces KIF5B clusters along axons of cultured cerebellar neurons. Cerebellar neurons were cultured from wild-type and *Kv3.1*$^{-/-}$ mouse pups (1–2 postnatal days) for 3 weeks. (**A**) Action potentials induced by a square-pulse current injection (1-second duration; 140 pA) from cultured cerebellar neurons (21 DIV) of wild-type (top) and Kv3.1 knockout (bottom) mice. (**B**) Waveforms of the 1st action potentials in A. (**C**) Input-output relationships of cultured cerebellar neurons from wild-type (circles) and Kv3.1 KO (triangles) mice. 2w, neurons before 2 weeks old (10–12 DIV); 3w, neurons around 3 weeks old (21 DIV). (**D**,**E**) Co-staining of endogenous KIF5 (green) and Kv3.1b (red) along axons of cultured cerebellar neurons from wild-type and *Kv3.1*$^{-/-}$ mice. (**F**) Endogenous KIF5B (green) and KLC1 (red) staining pattern in cultured wild-type cerebellar neurons at 20 DIV. (**G**) Endogenous KIF5B and KLC1 staining pattern in cultured Kv3.1 KO cerebellar neurons at 20 DIV. (**H**) To quantify the KIF5B clusters from the wild-type (left) and *Kv3.1*$^{-/-}$ (right) cerebellar neuron axons, images were thresholded and binarized to show pixel clusters. (**I**) Quantification of results shown in H. The number of experiments is indicated within the bars; **P*<0.05, ***P*<0.01 (*t*-test). Scale bars: 25 μm (D,E); 100 μm in (F,G), 15 μm (H).

vesicle. Although multiple kinesin motors to transport one carrier vesicle is accepted, the number of active kinesins is believed to be less than 10, supported by experiments and mathematical modeling (Erickson et al., 2011; Shubeita et al., 2008; Gazzola et al., 2009). In sharp contrast, despite all the caveats (Gu and Gu, 2010), our quantitative microscopy data suggest that in the presence of Kv3.1 one anterograde transporting vesicle can astonishingly contain up to 200 motor dimers (Fig. 8C). It is important to note that this number is obtained under the overexpression condition and may be close to the upper limit for a transporting vesicle. How many of these motors actively engage in walking along microtubules remains an open question. It is possible that many motors on the vesicle do not bind microtubules at the same time, but they may function as a reserve

pool to increase the processivity. The motors that actively engage in walking along microtubules can be further regulated by microtubule-binding proteins (Dixit et al., 2008). Nonetheless, this study has revealed a novel mechanism by which the motor number on a transporting vesicle can be effectively regulated. On the other hand, Kv3 channels may not be the only membrane proteins that can cluster kinesin motors. For instance, a recent study shows that Sunday Driver/JIP3 directly binds to KIF5 and activates the motor, but unlike Kv3, its oligomerization is not necessary, nor sufficient, for KIF5-mediated transport (Sun et al., 2011). Currently, it remains unclear whether JIP3 can also cluster KIF5 motors, which should depend on the nature of oligomerization. SNAP25 and VAMP2 can also form homo-dimers or hetero-oligomers, but both do not markedly activate and cluster KIF5 (Fig. 7).

Oligomerization of kinesin binding proteins (especially those membrane integral proteins that are embedded within transporting vesicles) regulating the motor number may be a general mechanism profoundly changing the motor function (supplementary material Fig. S4), in a way analogous to the cargo-mediated dimerization of other motor proteins (Tomishige et al., 2002; Sivaramakrishnan and Spudich, 2009; Yu et al., 2009).

Other potential mechanisms underlying KIF5 motor clustering

To determine how Kv3.1 deletion affects KIF5 clustering, we performed a series of experiments on Kv3.1 KO mice. Clear reduction of KIF5B clusters was observed, but clusters were still abundant in Kv3.1 KO neurons (Figs 9, 10). This may be due to the following reasons: (1) Other Kv3 channels, with highly conserved T1 domains, are present in cerebellum, including Kv3.3 and Kv3.4 channels. These channels can also cluster KIF5 due to the conserved T1 domains. (2) Besides Kv3 channels, there are unidentified proteins that can cluster KIF5 motors. Moreover, KIF5-mediated transport of Kv3 channels is a transient process. (3) Other mechanisms underlying KIF5 clustering, for instance, clustering of $KIF5B_{RKR}$-YFP may result from elimination of auto-inhibition (Fig. 6). However, it remains unclear what clusters $KIF5B_{RKR}$-YFP.

Physiological functions of clustering KIF5 motors

Axonal transport mediated by clustered KIF5 may be a unique way for some cargos riding motor proteins. Precise targeting of various ion channels to correct location is critical for neuronal excitability and synaptic transmission. How channel proteins are transported to the right neuronal compartments has been an outstanding question in neurobiology. Several ligand-gated ion channels, such as two major type of glutamate receptors (NMDA and AMPA receptors) and $GABA_A$ receptors, bind to kinesin motors via specific adaptor proteins (Barry and Gu, 2012). Since these adaptors are monomeric, or at least unlikely form multimeric complexes, loading of the channel proteins will not cluster the kinesin motors. Our studies have demonstrated a direct binding between Kv3.1 channels and KIF5 motors. Different from all other known channels that are transported by KIF5, Kv3.1 channels activates and clusters KIF5 motors, which itself may also be a novel mechanism ensuring the specificity of cargo transport.

Finally, mutations in Kv3.3 channel gene cause spinocerebellar ataxia with cerebellar atrophy (Waters et al., 2006). How does altered Kv3 channel activity lead to morphological changes in neural circuits remains an open question. A recent study shows that artificially clustered kinesin-1 can cause cilia-like beating of active microtubule bundles (Sanchez et al., 2011). Thus, clustered KIF5 motors can alter the behavior of microtubule tracks and indirectly affect the transport of other proteins. Therefore, our current and previous works showing Kv3 channels are linked to actin and microtubule cytoskeletons via ankyrin-G and KIF5, respectively (Xu et al., 2010; Xu et al., 2007), may shed light on this intriguing question. In particular, this work has raised a possibility that Kv3 channels may regulate axonal transport of other cargos via clustering kinesin-1, which is an interesting topic for further investigation.

Materials and Methods

cDNA constructs

GST-Tail, GST-T70 (GST-$Tail_{865–934}$), GST-T63 (GST-$Tail_{758–820}$), His-31T1, Kv3.1aHA, Kv3.1bHA, CFP-Kv3.1aHA, CFP-Kv3.1bHA, YFP-T70, YFP-T63, KIF5B-YFP were previously described (Xu et al., 2010; Gu et al., 2006; Xu et al., 2007). GST-$Tail_{865–986}$, GST-$Tail_{892–934}$, GST-$Tail_{870–896}$, GST-$Tail_{865–891}$, GST-$Tail_{892–912}$, GST-$Tail_{875–896}$, GST-$Tail_{913–934}$, GST-$Tail_{856–886}$, GST-$Tail_{892–929}$, GST-$Tail_{892–924}$, GST-$Tail_{897–934}$, GST-$Tail_{902–934}$, and GST-$Tail_{875–919}$ were made by inserting the PCRed cDNA fragments corresponding to the indicated regions of KIF5B tail into the pGEX4T-2 vector. GST-$T70_{RKR}$, YFP-$T70_{RKR}$, and $KIF5B_{RKR}$-YFP were made by mutating $R^{892}K^{893}R^{894}$ to DDD with Quickchange based on GST-T70, YFP-T70 and KIF5B-YFP, respectively. His-KLC1 and His-Motor were made by inserting the KLC1 full-length cDNA (OpenBiosystem, Huntsville, AL) and the cDNA containing KIF5B residues 1 to 399 into pRSET B vector. C(Y)FP-KLC1 was made by inserting the KLC1 full length cDNA into pEC(Y)FP-C1 (Clontech Laboratories, Inc., Mountain View, CA) between BlgII and *Hin*dIII. C(Y)FP-SNAP25 and C(Y)FP-VAMP2 were made by inserting the full length cDNAs into pEC(Y)FP-C1 between *Bgl*II and EcoR1. All constructs were confirmed by sequencing.

Antibodies and immunostaining

Antibodies used include mouse anti-6×His antibodies (Invitrogen, Carlsbad, CA; UC Davis/NIH NeuroMab facility (clone N144/14, Davis, CA), mouse anti-GST and anti-Kv3.1b antibodies (clone N100/13 and N16B/8, respectively; UC Davis/NIH NeuroMab Facility), mouse anti-β-tubulin and anti-KIF5 H2 antibodies (Millipore, Billerica, MA), mouse anti-GRIP1 antibody (Abcam, Cambridge, MA), rabbit polyclonal anti-microtubule-associated protein 2 (MAP2) and anti-Tau1 antibodies (Chemicon, Temecula, CA), rabbit polyclonal anti-Kv3.1b antibody (Alomone Labs, Jerusalem, Israel), rabbit polyclonal anti-KLC1 antibody (Santa Cruz Biotechnology Inc., Santa Cruz, CA), rabbit anti-SNAP25, anti-VAMP2 and anti-KIF5B antibodies (Abcam), rat monoclonal anti-HA antibody (Roche, Indianapolis, IN), Cy2, Cy3, and Cy5 conjugated secondary antibodies (Jackson ImmunoResearch Laboratories, West Grove, PA). The procedures of immunocytochemistry were described previously (Gu et al., 2006). In brief, the neurons were fixed with 4% formaldehyde (from 10% ultrapure EM grade and methonal free; Polysciences, Warrington, PA) and 4% sucrose in PBS for 20 minutes, and stained with specified antibodies under permeabilized conditions (in the presence of 0.2% Triton X100) to label total proteins. To distinguish axons and dendrites of neurons, an anti-Tau1 (Tau1 is an axonal marker) antibody or an anti-MAP2 (MAP2 is a dendritic marker) antibody was used in costaining. F-actin was labeled with phalloidin Alexa Fluor 546 and nuclei were stained with Hoechst 33342 (Invitrogen).

Hippocampal neuron culture and transfection

Hippocampal neuron culture was prepared as previously described from E18 rat embryos (Barry et al., 2010; Gu et al., 2012; Gu and Gu, 2010). In brief, 2 days after neuron plating, 1 μM cytosine arabinose (Sigma, St Louis, MO) was added to the neuronal culture medium to inhibit glial growth for the subsequent 2 days, then replaced with the normal culture medium. The culture medium was replenished twice a week by replacing half the volume. For transient transfection, neurons in culture at 5–7 DIV were incubated in Opti-MEM containing 0.8 μg of cDNA plasmid and 1.5 μl of Lipofectamine2000 (Invitrogen) for 20 minutes at 37℃.

Protein purification and *in vitro* binding assays

Expression of GST- or 6×His-tagged fusion proteins was induced in BL21 *E. coli* cells with 1 mM Isopropyl β-D-1-thiogalactopyranoside (IPTG) for 4 hours at 37℃. Bacterial pellets were solubilized with sonication in the pulldown buffer (50 mM Tris-HCl, pH 7.4, 150 mM NaCl, 1% Triton X-100, and a complete protease inhibitor tablet) at 4℃, and centrifuged at 50,000×***g*** for 30 minutes at

4℃. The supernatants were incubated either with glutathione beads (GE Healthcare Bio-Sciences AB, Sweden) or with Co^{2+} beads (TALON metal affinity resin, Clontech Laboratories Inc.) at 4℃ for 3 hours. After extensive washing, the beads were coated with purified fusion proteins and were eluted with the elution buffer containing either 20 mM glutathione or 150 mM imidazole. The elution was further dialyzed with the pulldown buffer at 4℃ overnight.

In binding assays to map the Kv3.1 T1-binding site in Fig. 2, glutathione beads coated with purified GST fusion proteins were further incubated with bacterial lysate supernatant containing His-31T1 at 4℃ for 2 hours. After extensive washing, the precipitants were eluted with 2× sample buffer, resolved in SDS-PAGE, and subjected to western blotting with an anti-His antibody.

In pulldown assays using purified proteins, purified GST fusion proteins (around 2.5–5 μg) were first coated onto glutathione beads (beads total volume: 30 μl). Coated beads were further incubated with purified His-tagged proteins in different molar ratios in the pulldown buffer without protease inhibitors (total volume 500 μl) at room temperature for 1 hour. After extensive washing, the precipitants were eluted with 2× sample buffer, resolved in SDS-PAGE, and subjected to western blotting or Colloidal Blue staining. In Fig. 3C, after binding, the beads were quickly washed once (~15 seconds) with the IP buffer and immediately incubated with the sample buffer. Each *in vitro* binding assay was performed at least three times.

Surface plasmon resonance experiments to measure binding affinities of protein–protein interactions

Surface plasmon resonance (SPR) experiments were performed at 25℃ on a Biacore T100 instrument (GE Healthcare, Piscataway, NJ) with CM5 sensor chips (GE Healthcare). One microgram of monoclonal anti-GST antibody was immobilized on flow cells covalently coupled as recommended by the manufacturer using the amine-coupling kit (GE Healthcare). Purified GST (0.6 μg) flowed over in the running buffer (50 mM Tris-HCl, pH 7.4, 150 mM NaCl) and was captured by the antibody in cell 1 as a control, and other GST fusion proteins (0.6 μg) were immobilized in cells 2–4. Purified His-31T1 at different concentrations was injected at a flow rate of 20 μl/minute for 180 seconds. After 300 seconds of dissociation, the chip was fully regenerated with 1 M NaCl for 600 seconds. All sensorgrams show data in which the background signal (GST in cell 1) was subtracted from the total signal (GST fusion proteins). The K_d for His-31T1 binding to GST fusion proteins were calculated by either fitting the curves to obtain K_{on} and K_{off} (for GST-T70) or plotting saturation binding curves using the equilibrium response value at the plateau of all curves (for GST-$Tail_{892–934}$). Since we estimated the binding stoichiometry of GST-T70 and His-31T1 is about 1:1 (therefore 4:4), in analyzing SPR experimental data we adopted the ratio 1:1, assuming no allosteric effect during binding.

Microtubule assembly and binding assays

To reconstitute microtubule *in vitro*, purified tubulin (Sigma) (20 μl in 2 mg/ml) was incubated in the polymerization buffer containing 80 mM PIPES (N,N0-piperazine diethane sulfonic acid), pH 6.9, 0.5 mM $MgCl_2$, 1 mM GTP (guanosine-50-triphosphate), and 5% glycerol, at 37℃ for 30 minutes. Then purified proteins (around 5 μg) were added and incubated for another 30 minutes. Microtubules and binding proteins were pelleted at 50,000×***g*** for 30 minutes at room temperature and resuspended in sample buffer. To determine the amounts of tubulin and other protein in the microtubule or supernatant fractions, 15 μl of supernatants and resuspended pellets were analyzed by SDS-PAGE. In the competition experiment of GST-T70 and His-31T1, 100 μM paclitaxel was added to promote and stabilize microtubule formation.

Fluorescence microscopy and quantification

Fluorescence images were captured with a Spot CCD camera RT slider (Diagnostic Instrument Inc., Sterling Heights, MI) in a Zeiss upright microscope, Axiophot, using Plan Apo objectives 20× /0.75 and 100× /1.4 oil, saved as 16-bit TIFF files, and analyzed with NIH Image J and Sigmaplot 10.0 for fluorescence intensity quantification. Exposure times were controlled so that the pixel intensities in dendrites and axons were below saturation, but the same exposure time was used within each group of an experiment. The quantification procedure was described previously (Xu et al., 2010). Only transfected neurons with clearly separated dendrites and axons, and isolated from other transfected cells, were chosen for analysis. Using NIH Image J, we laid a line along the major axon to acquire its average fluorescence intensity (in arbitrary unit) ($\boldsymbol{F_{axon}}$), and laid lines along proximal dendrites which connect with soma to obtain the average fluorescence intensity of the somatodendritic region ($\boldsymbol{F_{sd}}$) to represent the total level. Thus, the ratio ($\boldsymbol{F_{axon}/F_{sd}}$) reflects the relative axonal level. The background fluorescence intensity was measured for each image and subtracted.

Live cell and FRET imaging

Neurons growing on 25 mm coverslips were loaded into the imaging chamber (Molecular Devices, Downingtown, PA) and incubated with imaging buffer (HE-LF medium (Brainbits, Springfield, IL) plus 2% B-27, 0.5 mM glutamine, and 25 μM glutamate) at room temperature. The timelapse imaging setup was built upon a Nikon (Nikon Inc., Melville, NY) TE2000 inverted microscope. Images were captured with a CCD camera Coolsnap HQ (Photometrics, Tucson, AZ) through CFP or YFP filter sets with 1 second exposure time. The filters were changed through filter wheels controlled through Lamda 10-3 (Sutter Instrument, Novato, CA) by MetaMorph software (Molecular Devices). The time-lapse imaging was performed with 2-second interval for 100 frames.

Our FRET imaging is used to detect sensitized emission, suitable for studying protein–protein interactions in living cells with a conventional fluorescence microscope. The strategy and protocol of FRET imaging were described previously in detail (Xu et al., 2010; Gu et al., 2001; Gu et al., 2006). In brief, three images were acquired sequentially through (1) YFP filter (excitation 500/20 nm, emission 535/20 nm); (2) CFP filter (emission 430/25 nm, emission 470/30 nm); (3) FRET filter set (excitation 430/25 nm, emission 535/30 nm). A single dichroic mirror [86004BS; Chroma (Chroma Technology Corp, Bellows Falls, VT)] was used with all three filter channels. FRET between CFP and YFP was measured and calculated for the entire image on a pixel-by-pixel basis by a three-filter 'microFRET' method. The raw FRET images consisted of both FRET and non-FRET components (the donor and acceptor fluorescence bleeding through the FRET filter). The extent of crossbleeding was characteristic of the particular optical system and determined by the use of cells that express either CFP- or YFP-fusion protein alone. Background fluorescence values were subtracted from each image before calculation. In our system, 64.7%±0.5% (n=18) of CFP, and 1.47%±0.08% (n=12) of YFP fluorescence bleed through the FRET channel, which were measured previously (Xu et al., 2010). We measured the ratio of crossbleeding for all the CFP- and YFP-fusion proteins used in this study. The ratio values are consistent with those obtained in previous studies. Therefore, $FRET_{corrected}=FRET_{raw}-(0.65\times CFP)-(0.015\times YFP)$. The calculation of $FRET_{corrected}$ was performed with the MetaMorph software.

Timelapse live-cell imaging and quantification of mobile puncta along axons

All measurements were carried out on kymographs made with the MetaMorph program as previous described (Gu and Gu, 2010). The total time for each movie is 198 seconds. We calculated the frequency of transport events (or the average number of moving puncta per movie) F(number/minute)=n/(198 seconds/60 seconds/minute). For instance, if one moving punctum (n=1) is observed in one movie (total 3.3 minutes long), F equals 0.3. F equals 0 if no moving punctum was seen in a movie. F equals 0.6 or 0.9 if 2 or 3 moving puncta were seen, respectively. Anterograde and retrograde puncta were presented as '+' and '−' values.

Using quantitative microscopy to estimate KIF5B-YFP motors in axonal puncta

We used five yeast strains (wild type and the ones expressing Arc1-mYFP, Arp2-mYFP, Fim1-mYFP, and Spn4-mYFP) (Wu and Pollard, 2005) to calibrate our quantitative microscope system as previously described (Gu and Gu, 2010). The fluorescence intensities measured in our microscope system were largely in a linear relationship with the published numbers (Gu and Gu, 2010). They were used to obtain the linear regression curve in SigmaPlot 11. $F_{total}=4.95n+61$. $R^2=0.96$. In the regression, four points with 0 (F_{total}) and 0 (n) were added to force the curve to get close to the zero point. Fluorescence intensities of KIF5B-YFP puncta were measured. The estimated number of YFP-fused motors (n) and the number of motor dimers (n/2) were calculated for each punctum.

Kv3.1 knockout mouse genotyping

Kv3.1 knockout (KO) mouse line was kindly provided by Dr R. Joho at UT Southwestern Medical Center and have been maintained using a PCR-based genotyping procedure as previously described (Ho et al., 1997; Sánchez et al., 2000; Hurlock et al., 2009). The Kv3.1 KO mice were backcrossed with BL6 for ten generations. Seizure can be observed occasionally from some Kv3.1 homozygotes (−/−) but not heterozygotes (+/−) mice. The following primers were used: forward primer 31F775 (for both WT and knockout, 5′-GCG CTT CAA CCC CAT CGT GAA CAA GA-3′), reverse primer 31R991 (for WT, 5′-GGC CAC AAA GTC AAT GAT ATT GAG GG-3′), and reverse primer PNR278 (for knockout, 5′-CTA CTT CCA TTT GTC ACG TCC TGC AC-3′). Three Kv3.1 KO (−/−) and three control Bl6 mice of either sex at the age of 2–4 months were used in the immunofluorescence study.

Immunofluorescence staining on mouse brain sections and cluster quantification

After cardiac perfusion and tissue fixation, mouse cerebellum was removed, post-fixed, and then embedded in optimal cutting temperature media (Sakura Finetek USA, Inc., Torrance, CA) and stored at −80℃ until sectioning. Coronal sections (40-μm thickness) of mouse cerebellum were cut with a Microm HM550 cryostat (Thermo Scientific, Waltham, MA) and collected on Superfrost Plus microscope slides (FisherScientific, Pittsburgh, PA). Immunostaining and imaging were performed as previously described (Jukkola et al., 2012). The whole images

captured with a 40× objective lens were processed for quantification using Metamorph by flattening the background, thresholding the images to include only the 5% highest intensity pixels, and binarizing the image. Kif5B puncta were quantified in ImageJ using the 'Analyze Particles' tool to count all pixel clusters ranging in size from 9–300 pixels.

Whole-cell patch clamp recording on cultured cerebellar neurons from wild-type and Kv3.1 KO mice

Current clamp recording of action potentials from cultured neurons was previously described (Gu et al., 2012). In brief, cerebellar neurons cultured from either WT or Kv3.1 KO mice, were recorded in two time windows, 2w (before 14 DIV; 10–12 DIV) and 3w (around 21 DIV; from 19–22 DIV). Neurons' membrane resistance, capacitance, and resting membrane potentials were measured. These values are consistent within each age group. Action potentials were induced by current injections (1000-ms duration; from 5 to 145 pA with increments of 10 pA) via the recording pipette. The studies were performed with three rounds of cultures. Each round had 4 to 6 pups.

Quantification of KIF5B clusters along axons of cultured cerebellar neurons from wild-type and Kv3.1 KO mice

The quantification procedure for KIF5B clusters along axons of cultured cerebellar axons is similar to that for cerebellar sections. All images captured with a 20× objective lens were processed for quantification using Metamorph by flattening the background, thresholding the images to include only the 5% highest intensity pixels, and binarizing the image. Kif5B puncta ranging in size from 9–300 pixels along axons (around 250 µm segments) were quantified in ImageJ.

Acknowledgements

We thank L. Wei for advice on statistical analysis, X. Li for technical assistance and R. Joho at UT Southwestern Medical Center for Kv3.1 KO mice.

Author contributions

J.B., M.X., Y.G., P.J. and C.S. performed the experiments and analyzed the data. A.D. helped with the SPR experiment. C.G. supervised the project, designed and performed experiments, and wrote the paper.

Funding

This work was supported by a grant from the National Institutes of Health, National Institute of Neurological Disorders and Stroke (NIH/NINDS) [grant number R01NS062720] to C.G. All animal experiments were conducted in accordance with the NIH Animal Use Guidelines. Deposited in PMC for release after 12 months.

Supplementary material available online at
http://jcs.biologists.org/lookup/suppl/doi:10.1242/jcs.122234/-/DC1

References

Andrews, S. B., Gallant, P. E., Leapman, R. D., Schnapp, B. J. and Reese, T. S. (1993). Single kinesin molecules crossbridge microtubules in vitro. *Proc. Natl. Acad. Sci. USA* **90**, 6503-6507.

Barry, J. and Gu, C. (2012). Coupling mechanical forces to electrical signaling: molecular motors and intracellular transport of ion channels. *Neuroscientist* [Epub ahead of print] doi: 10.1177/1073858412456088.

Barry, J., Gu, Y. and Gu, C. (2010). Polarized targeting of L1-CAM regulates axonal and dendritic bundling in vitro. *Eur. J. Neurosci.* **32**, 1618-1631.

Bean, B. P. (2007). The action potential in mammalian central neurons. *Nat. Rev. Neurosci.* **8**, 451-465.

Bi, G. Q., Morris, R. L., Liao, G., Alderton, J. M., Scholey, J. M. and Steinhardt, R. A. (1997). Kinesin- and myosin-driven steps of vesicle recruitment for Ca2+-regulated exocytosis. *J. Cell Biol.* **138**, 999-1008.

Bixby, K. A., Nanao, M. H., Shen, N. V., Kreusch, A., Bellamy, H., Pfaffinger, P. J. and Choe, S. (1999). Zn2+-binding and molecular determinants of tetramerization in voltage-gated K+ channels. *Nat. Struct. Biol.* **6**, 38-43.

Block, S. M., Goldstein, L. S. and Schnapp, B. J. (1990). Bead movement by single kinesin molecules studied with optical tweezers. *Nature* **348**, 348-352.

Burack, M. A., Silverman, M. A. and Banker, G. (2000). The role of selective transport in neuronal protein sorting. *Neuron* **26**, 465-472.

Cai, Q., Gerwin, C. and Sheng, Z. H. (2005). Syntabulin-mediated anterograde transport of mitochondria along neuronal processes. *J. Cell Biol.* **170**, 959-969.

Cai, D., Hoppe, A. D., Swanson, J. A. and Verhey, K. J. (2007). Kinesin-1 structural organization and conformational changes revealed by FRET stoichiometry in live cells. *J. Cell Biol.* **176**, 51-63.

Choe, S. (2002). Potassium channel structures. *Nat. Rev. Neurosci.* **3**, 115-121.

Coy, D. L., Hancock, W. O., Wagenbach, M. and Howard, J. (1999). Kinesin's tail domain is an inhibitory regulator of the motor domain. *Nat. Cell Biol.* **1**, 288-292.

Cross, R. and Scholey, J. (1999). Kinesin: the tail unfolds. *Nat. Cell Biol.* **1**, E119-E121.

Diefenbach, R. J., Mackay, J. P., Armati, P. J. and Cunningham, A. L. (1998). The C-terminal region of the stalk domain of ubiquitous human kinesin heavy chain contains the binding site for kinesin light chain. *Biochemistry* **37**, 16663-16670.

Dixit, R., Ross, J. L., Goldman, Y. E. and Holzbaur, E. L. (2008). Differential regulation of dynein and kinesin motor proteins by tau. *Science* **319**, 1086-1089.

Erickson, R. P., Jia, Z., Gross, S. P. and Yu, C. C. (2011). How molecular motors are arranged on a cargo is important for vesicular transport. *PLOS Comput. Biol.* **7**, e1002032.

Friedman, D. S. and Vale, R. D. (1999). Single-molecule analysis of kinesin motility reveals regulation by the cargo-binding tail domain. *Nat. Cell Biol.* **1**, 293-297.

Gazzola, M., Burckhardt, C. J., Bayati, B., Engelke, M., Greber, U. F. and Koumoutsakos, P. (2009). A stochastic model for microtubule motors describes the in vivo cytoplasmic transport of human adenovirus. *PLOS Comput. Biol.* **5**, e1000623.

Glater, E. E., Megeath, L. J., Stowers, R. S. and Schwarz, T. L. (2006). Axonal transport of mitochondria requires milton to recruit kinesin heavy chain and is light chain independent. *J. Cell Biol.* **173**, 545-557.

Grigg, J. J., Brew, H. M. and Tempel, B. L. (2000). Differential expression of voltage-gated potassium channel genes in auditory nuclei of the mouse brainstem. *Hear. Res.* **140**, 77-90.

Gu, C. and Barry, J. (2011). Function and mechanism of axonal targeting of voltage-sensitive potassium channels. *Prog. Neurobiol.* **94**, 115-132.

Gu, Y. and Gu, C. (2010). Dynamics of Kv1 channel transport in axons. *PLoS ONE* **5**, e11931.

Gu, C., Sorkin, A. and Cooper, D. M. (2001). Persistent interactions between the two transmembrane clusters dictate the targeting and functional assembly of adenylyl cyclase. *Curr. Biol.* **11**, 185-190.

Gu, C., Zhou, W., Puthenveedu, M. A., Xu, M., Jan, Y. N. and Jan, L. Y. (2006). The microtubule plus-end tracking protein EB1 is required for Kv1 voltage-gated K+ channel axonal targeting. *Neuron* **52**, 803-816.

Gu, Y., Barry, J., McDougel, R., Terman, D. and Gu, C. (2012). Alternative splicing regulates kv3.1 polarized targeting to adjust maximal spiking frequency. *J. Biol. Chem.* **287**, 1755-1769.

Hackney, D. D. and Stock, M. F. (2000). Kinesin's IAK tail domain inhibits initial microtubule-stimulated ADP release. *Nat. Cell Biol.* **2**, 257-260.

Hirokawa, N. and Takemura, R. (2005). Molecular motors and mechanisms of directional transport in neurons. *Nat. Rev. Neurosci.* **6**, 201-214.

Hirokawa, N., Sato-Yoshitake, R., Kobayashi, N., Pfister, K. K., Bloom, G. S. and Brady, S. T. (1991). Kinesin associates with anterogradely transported membranous organelles in vivo. *J. Cell Biol.* **114**, 295-302.

Ho, C. S., Grange, R. W. and Joho, R. H. (1997). Pleiotropic effects of a disrupted K+ channel gene: reduced body weight, impaired motor skill and muscle contraction, but no seizures. *Proc. Natl. Acad. Sci. USA* **94**, 1533-1538.

Howard, J., Hudspeth, A. J. and Vale, R. D. (1989). Movement of microtubules by single kinesin molecules. *Nature* **342**, 154-158.

Huang, J. D., Brady, S. T., Richards, B. W., Stenolen, D., Resau, J. H., Copeland, N. G. and Jenkins, N. A. (1999). Direct interaction of microtubule- and actin-based transport motors. *Nature* **397**, 267-270.

Hurlock, E. C., Bose, M., Pierce, G. and Joho, R. H. (2009). Rescue of motor coordination by Purkinje cell-targeted restoration of Kv3.3 channels in Kcnc3-null mice requires Kcnc1. *J. Neurosci.* **29**, 15735-15744.

Jahng, A. W., Strang, C., Kaiser, D., Pollard, T., Pfaffinger, P. and Choe, S. (2002). Zinc mediates assembly of the T1 domain of the voltage-gated K channel 4.2. *J. Biol. Chem.* **277**, 47885-47890.

Jan, L. Y. and Jan, Y. N. (1997). Cloned potassium channels from eukaryotes and prokaryotes. *Annu. Rev. Neurosci.* **20**, 91-123.

Jukkola, P. I., Lovett-Racke, A. E., Zamvil, S. S. and Gu, C. (2012). K+ channel alterations in the progression of experimental autoimmune encephalomyelitis. *Neurobiol. Dis.* **47**, 280-293.

Kaczmarek, L. K., Bhattacharjee, A., Desai, R., Gan, L., Song, P., von Hehn, C. A., Whim, M. D. and Yang, B. (2005). Regulation of the timing of MNTB neurons by short-term and long-term modulation of potassium channels. *Hear. Res.* **206**, 133-145.

Konishi, Y. and Setou, M. (2009). Tubulin tyrosination navigates the kinesin-1 motor domain to axons. *Nat. Neurosci.* **12**, 559-567.

Laib, J. A., Marin, J. A., Bloodgood, R. A. and Guilford, W. H. (2009). The reciprocal coordination and mechanics of molecular motors in living cells. *Proc. Natl. Acad. Sci. USA* **106**, 3190-3195.

Leopold, P. L., McDowall, A. W., Pfister, K. K., Bloom, G. S. and Brady, S. T. (1992). Association of kinesin with characterized membrane-bounded organelles. *Cell Motil. Cytoskeleton* **23**, 19-33.

Li, M., Jan, Y. N. and Jan, L. Y. (1992). Specification of subunit assembly by the hydrophilic amino-terminal domain of the Shaker potassium channel. *Science* **257**, 1225-1230.

Long, S. B., Campbell, E. B. and Mackinnon, R. (2005). Crystal structure of a mammalian voltage-dependent Shaker family K+ channel. *Science* **309**, 897-903.

Maniar, T. A., Kaplan, M., Wang, G. J., Shen, K., Wei, L., Shaw, J. E., Koushika, S. P. and Bargmann, C. I. (2012). UNC-33 (CRMP) and ankyrin organize microtubules and localize kinesin to polarize axon-dendrite sorting. *Nat. Neurosci.* **15**, 48-56.

Miller, R. H. and Lasek, R. J. (1985). Cross-bridges mediate anterograde and retrograde vesicle transport along microtubules in squid axoplasm. *J. Cell Biol.* **101**, 2181-2193.

Nakata, T., Niwa, S., Okada, Y., Perez, F. and Hirokawa, N. (2011). Preferential binding of a kinesin-1 motor to GTP-tubulin-rich microtubules underlies polarized vesicle transport. *J. Cell Biol.* **194**, 245-255.

Puente, N., Mendizabal-Zubiaga, J., Elezgarai, I., Reguero, L., Buceta, I. and Grandes, P. (2010). Precise localization of the voltage-gated potassium channel subunits Kv3.1b and Kv3.3 revealed in the molecular layer of the rat cerebellar cortex by a pre-embedding immunogold method. *Histochem. Cell Biol.* **134**, 403-409.

Rudy, B. and McBain, C. J. (2001). Kv3 channels: voltage-gated K+ channels designed for high-frequency repetitive firing. *Trends Neurosci.* **24**, 517-526.

Rudy, B., Chow, A., Lau, D., Amarillo, Y., Ozaita, A., Saganich, M., Moreno, H., Nadal, M. S., Hernandez-Pineda, R., Hernandez-Cruz, A. et al. (1999). Contributions of Kv3 channels to neuronal excitability. *Ann. N. Y. Acad. Sci.* **868**, 304-343.

Sánchez, J. A., Ho, C. S., Vaughan, D. M., Garcia, M. C., Grange, R. W. and Joho, R. H. (2000). Muscle and motor-skill dysfunction in a K+ channel-deficient mouse are not due to altered muscle excitability or fiber type but depend on the genetic background. *Pflugers Arch.* **440**, 34-41.

Sanchez, T., Welch, D., Nicastro, D. and Dogic, Z. (2011). Cilia-like beating of active microtubule bundles. *Science* **333**, 456-459.

Schnitzer, M. J. and Block, S. M. (1997). Kinesin hydrolyses one ATP per 8-nm step. *Nature* **388**, 386-390.

Setou, M., Seog, D. H., Tanaka, Y., Kanai, Y., Takei, Y., Kawagishi, M. and Hirokawa, N. (2002). Glutamate-receptor-interacting protein GRIP1 directly steers kinesin to dendrites. *Nature* **417**, 83-87.

Shubeita, G. T., Tran, S. L., Xu, J., Vershinin, M., Cermelli, S., Cotton, S. L., Welte, M. A. and Gross, S. P. (2008). Consequences of motor copy number on the intracellular transport of kinesin-1-driven lipid droplets. *Cell* **135**, 1098-1107.

Sivaramakrishnan, S. and Spudich, J. A. (2009). Coupled myosin VI motors facilitate unidirectional movement on an F-actin network. *J. Cell Biol.* **187**, 53-60.

Sobotzik, J. M., Sie, J. M., Politi, C., Del Turco, D., Bennett, V., Deller, T. and Schultz, C. (2009). AnkyrinG is required to maintain axo-dendritic polarity in vivo. *Proc. Natl. Acad. Sci. USA* **106**, 17564-17569.

Song, A. H., Wang, D., Chen, G., Li, Y., Luo, J., Duan, S. and Poo, M. M. (2009). A selective filter for cytoplasmic transport at the axon initial segment. *Cell* **136**, 1148-1160.

Sun, F., Zhu, C., Dixit, R. and Cavalli, V. (2011). Sunday Driver/JIP3 binds kinesin heavy chain directly and enhances its motility. *EMBO J.* **30**, 3416-3429.

Tomishige, M., Klopfenstein, D. R. and Vale, R. D. (2002). Conversion of Unc104/KIF1A kinesin into a processive motor after dimerization. *Science* **297**, 2263-2267.

Twelvetrees, A. E., Yuen, E. Y., Arancibia-Carcamo, I. L., MacAskill, A. F., Rostaing, P., Lumb, M. J., Humbert, S., Triller, A., Saudou, F., Yan, Z. et al. (2010). Delivery of GABAARs to synapses is mediated by HAP1-KIF5 and disrupted by mutant huntingtin. *Neuron* **65**, 53-65.

Vershinin, M., Carter, B. C., Razafsky, D. S., King, S. J. and Gross, S. P. (2007). Multiple-motor based transport and its regulation by Tau. *Proc. Natl. Acad. Sci. USA* **104**, 87-92.

Waters, M. F., Minassian, N. A., Stevanin, G., Figueroa, K. P., Bannister, J. P., Nolte, D., Mock, A. F., Evidente, V. G., Fee, D. B., Müller, U. et al. (2006). Mutations in voltage-gated potassium channel KCNC3 cause degenerative and developmental central nervous system phenotypes. *Nat. Genet.* **38**, 447-451.

Weiser, M., Vega-Saenz de Miera, E., Kentros, C., Moreno, H., Franzen, L., Hillman, D., Baker, H. and Rudy, B. (1994). Differential expression of Shaw-related K+ channels in the rat central nervous system. *J. Neurosci.* **14**, 949-972.

Wong, Y. L. and Rice, S. E. (2010). Kinesin's light chains inhibit the head- and microtubule-binding activity of its tail. *Proc. Natl. Acad. Sci. USA* **107**, 11781-11786.

Wu, J. Q. and Pollard, T. D. (2005). Counting cytokinesis proteins globally and locally in fission yeast. *Science* **310**, 310-314.

Xu, J., Yu, W., Jan, Y. N., Jan, L. Y. and Li, M. (1995). Assembly of voltage-gated potassium channels. Conserved hydrophilic motifs determine subfamily-specific interactions between the alpha-subunits. *J. Biol. Chem.* **270**, 24761-24768.

Xu, M., Cao, R., Xiao, R., Zhu, M. X. and Gu, C. (2007). The axon-dendrite targeting of Kv3 (Shaw) channels is determined by a targeting motif that associates with the T1 domain and ankyrin G. *J. Neurosci.* **27**, 14158-14170.

Xu, M., Gu, Y., Barry, J. and Gu, C. (2010). Kinesin I transports tetramerized Kv3 channels through the axon initial segment via direct binding. *J. Neurosci.* **30**, 15987-16001.

Yu, C., Feng, W., Wei, Z., Miyanoiri, Y., Wen, W., Zhao, Y. and Zhang, M. (2009). Myosin VI undergoes cargo-mediated dimerization. *Cell* **138**, 537-548.